October 31, 2005

Seismic Evaluation of Hydrocarbon Saturation in Deep-Water Reservoirs

Grant/Cooperative Agreement DE-FC26-02NT15342.

QUARTERLY REPORT

Report Period Start Date: July 1, 2005
Report period End Date: September 30, 2005

Primary Author: Dr. Michael Batzle

Prime Contractor: Colorado school of Mines
Department of Geophysics
1500 Illinois St.
Golden, Colorado 80401

Subcontractors: University of Houston
Texas A&M University

Industrial Collaborators: Paradigm, Veritas

Principal Investigators:

M. Batzle - Colorado School of Mines
D-h Han - University of Houston (formerly: Houston Advanced Research Center)
R. Gibson - Texas A&M University
Huw James - Paradigm Geophysical

Disclaimer

Abstract

During this last quarter of the "Seismic Evaluation of Hydrocarbon Saturation in Deep-Water Reservoirs" project (Grant/Cooperative Agreement DE-FC26-02NT15342), we have moved forward on several fronts, including data acquisition as well as analysis and application.

During this quarter we have:

Completed our site selection (finally).
Measured fluid effects in Troika deep water sand sample

- Applied the result to Ursa 'fizz gas' zone
- Compared thin layer property averaging on AVO response
- Developed target oriented NMO stretch correction
- Examined thin bed effects on A-B crossplots

Begun incorporating outcrop descriptive models in seismic forward models
Several factors can contribute to limit our ability to extract accurate hydrocarbon saturations in deep water environments. Rock and fluid properties are one factor, since, for example, hydrocarbon properties will be considerably different with great depths (high pressure) when compared to shallow properties. Significant over pressure, on the other hand will make the rocks behave as if they were shallower. In addition to the physical properties, the scale and tuning will alter our hydrocarbon indicators. Reservoirs composed of thin bed effects will broaden the reflection amplitude distribution with incident angle. Normal move out (NMO) stretch corrections based on frequency shifts can be applied to offset this effect. Tuning will also disturb the location of extracted amplitudes on AVO intercept and gradient (A-B) plots. Many deep water reservoirs fall this tuning thickness range. Our goal for the remaining project period is to systematically combine and document these various effects for use in deep water exploration.

Contents

Figures

Tables

Equations

Results and Discussion

Test Sites

As will be seen in this report, we have begun detailed analysis on data from several of our target sites. Data and samples had to be acquired from several sources and the process is still incomplete (see Table 1 below). Seismic data has been obtained from Mobil, TGS, and the ERCH consortium. Samples were obtained from Kerr-McGee and Marathon Oil Companies. We are now progressing with the analysis of several of the selected sites.

Field	Attribute	Status
Nansen	Core samples & logs available	Seismic Obtained, Samples
Viking	Mobil North Sea data with logs	Seismic data and logs acquired
Ursa	Multiple real and false HCI	Seismic analysis begun
Troika	Some data already published	Samples Prep., Veritas 2-D line,
Mars	Published data, salt confined	Veritas 2-D lines, Logs obtained
Boomvang	Near Nansen (Kerr-McGee)	Samples & logs obtained
Mensa	Structurally simple, deep water	Veritas 2-D line, Logs acquired
Teal South	Shelf, only one well, data available	Post-stack data and logs at TAMU

Table 1. Current status of candidate Deep-water Gulf of Mexico Fields with seismic hydrocarbon indicators

The Teal South data had some arbitrary gains and other inappropriate processing performed which render the data of limited value. These data can be used for examples, but complete reprocessing is not practical. The research staff at Veritas is still negotiating with their marine group to obtain the Troika, Mars and Mensa data. The specific lines requested were shown in a previous quarterly report

Deep Water Geology

Deep water deposits are those that have been deposited in water depths considered to be deep that are in the upper to middle slope region of a basin. (Weimer & Slatt, 2004) Turbidites are sediments that a carried by marine sediment gravity flows caused by turbidity currents. We must distinguish between engineering deepwater and geologic deepwater definitions. Engineering definition specifies drilling depths greater than 500m-2000 m where as geologic deepwater refers to deposits in deep water environments. Turbidite sequences or Bouma sequences are defined as fining upward sequences. (Bouma, 2004) It is important to note that geologic outcrop observations and deepwater data have some differences in terms of the geologic depositional environment therefore some of the features or patterns that occur may be different due to this. Confined turbidite systems are those deepwater systems whose development has been constrained by pronounced basin floor topography. In an unconfined setting the sediments would be free to spread radially across the ocean floor. (Lomas & Joseph, 2004)
The Permian Delaware basin brushy Canyon Formation turbidite system in West Texas-New Mexico is a different type of system. (Gardner & Borer, 2000) (Carr & Gardner, 2000) The Brushy Canyon formation is a sand rich system with very little sand and is unconfined. The system is an example of an aeolian transport system across shelf to outer reef shelf zone and the deep-water deposits moved through holes in reef to deep water. Figure 1 shows a schematic view of one brushy canyon fan conduit and illustrates cycles of erosion, bypass and channelization due to sediment gravity flows. (Gardner et al, 2005)

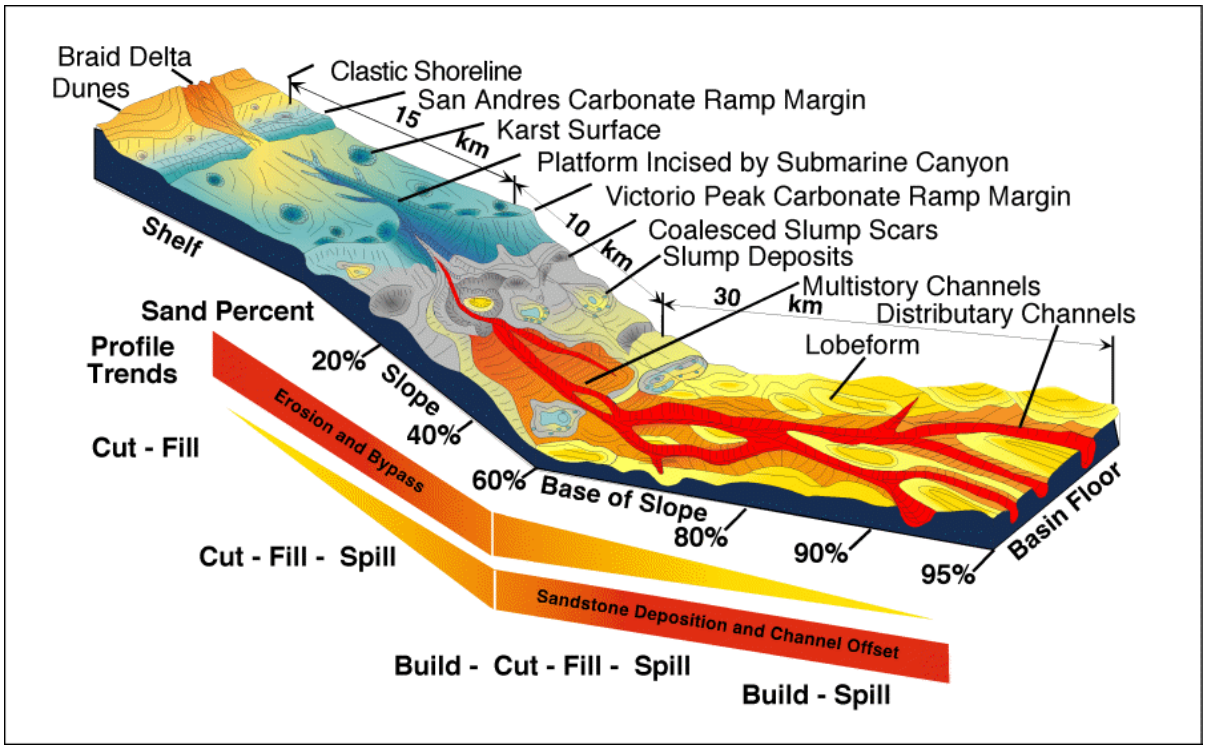

Figure 1. Schematic depiction of changing architectural styles and depositional patterns inferred along the slope and basin profile of one Brushy Canyon fan conduit (Gardner et al, 2005)

Mars–Ursa Intraslope basin, like many other deep-water basins in the Northern Gulf of Mexico, is characterized as a diapiritic Intraslope basin meaning that salt diapirism is an active tectonic force. These features can cause obstruction of sediment flow pathways, which results in a confined basin setting (Bouma, 2004). Many of the basins are too small to accomodate amount of sediment being flowing in therefore basins fill up (ponding) and tend to overflow to locate a place where they can easily bypass sediments. Resulting facies that form in these areas tend to be non-amalgamated channels, amalgamated channels, sheet sands, condensed section, and slump/slope deposits. Figure 2 shows a schematic of the ponding and bypass stages of turbidite flows in the Mars-Ursa Intraslope basin.

Some of the basic turbidite elements that are commonly found in both confined and unconfined settings are, erosional features (excluding channels), erosional and aggradational channels, overbank deposits, channel lobe transitions that include sheets, basin floor fans, and low stand fans. The most important facies for reservoir characterization are, thin bed levees, sheet sands and channels. (Chapin et. al., 1994)

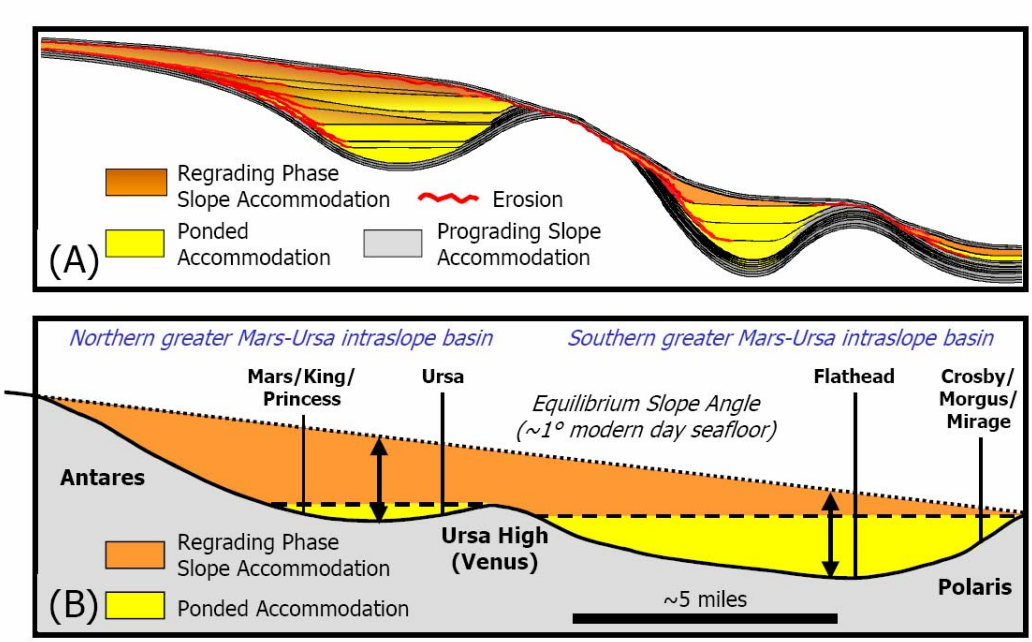

Figure 2. Confined basin setting schematic shows ponded accommodation and bypass as well as erosional features in the Mars-Ursa Intraslope Basin (Meckel et. al., 2002)

Previous Work

The paper entitled 'Genetic Stratigraphy, Stratigraphic Architecture, and reservoir Stacking Patterns of Upper Miocene-Lower Pliocene greater Mars-Ursa Intraslope Basin Mississippi canyon Gulf of Mexico' has been instrumental in the understanding of the Ursa basin and will help to compensate for our lack of 3-D seismic data when trying to predict the influence of geology on the seismic signature and occurrence of DHI's. It will also be helpful to compare the unconfined basin setting of deepwater play to confined setting and identify the difference and similarities that can influence DHI's. Another work that has helped in the understanding of the field is Fred Hilterman's Seismic Amplitude Interpretation (2001). Hilterman's studies of DHI's in the Ursa field and some of the interpretation from his book was used as the basis for the following work. In addition, Prather et al. developed a classification for lithologic calibration and Stratigraphic Succession of Seismic facies of Intraslope basins deep water Gulf of Mexico, and this was used as a basis to understand the geologic influence of deepwater geologic features on seismic facies.

Using outcrops as analogs for reservoir characterization is a well developed idea. Examples include Brown and Slatt (1997) who used outcrops to design simulation models, Sullivan et.al. (2004) used outcrops to characterize and constrain deep water reservoir geometries for Diana Field, western Gulf of Mexico. Also, IFP held a conference in April 1992 in Scarborough on Subsurface reservoir Characterization from outcrop observations. We will build on this by demonstrating how deep-water lithologies

and geometries impact seismic response and control fluid placement and compartmentalization.

Stratigraphic Interpretation of Ursa Basin

The geologic framework of the Mars-Ursa Intraslope was adapted from the stratigraphic interpretation from Meckel et. al. (2002). The basin is composed of cyclic deposition of couplets of sheet sands and channelized or amalgamated systems bounded by condensed section. The sheet sands and channel systems are separated by bypass erosion or evulsion surfaces. These couplets form 4th order cycles, and according to Meckel et. al. are the building blocks for seismic facies assemblages that are on the 3rd order scale. These assemblages follow the fill spill patterns characteristic of the mini basin setting. Condensed sections form from pelagic sediments falling out of the water column and can be associated with abrupt changes in overpressure. (Meckel et. al., 2002) The main facies that we will focus on are sheets sands, amalgamated channels, no amalgamated channels and condensed section. Definitions of deepwater elements have been agreed upon by various experts in the field and summarized in Petroleum Systems of deepwater settings. (Slatt &Weimer, 2003)

- *Depositional Lobes* (Mutti and Normark, 1987,1991): areas of sand deposition that are located downslope from the main channel. They can be characterized to have tabular geometry, have thicknesses generally 3-15 m and they are usually made up of coarse sandstone beds that are parallel sided.

- *Sheet* (Mahaffie, 1994): fan lobe deposits that are laterally continuous, tabular geometry. They can be amalgamated or non-amalgamated (layered) where amalgamated sheets are high net/gross stacked assemblages of top absent Bouma sequences and layered sheets are lower net/gross with complete Bouma sequences.

- *Channel* (Mutti and Normark, 1991): Elongate negative relief features produced &/or maintained by turbidity current flow. They represent long-term pathways of sediments transport. The shape and position of the channel within a system are controlled by depositional processes or erosional downcutting. Channels can be amalgamated or clustered together or they can be non-amalgamated or totally isolated. (Anderson, 2005)

- *Overbank* (Mutti and Normark, 1991): fine grained to thin bedded turbidite sediments that can be laterally extensive and are adjacent to main channels in a turbidite system and can consist of two parts 1) those with levee relief and 2) those without relief

- *Thin beds* (Shew et. al., 1994): thin beds are interpreted to include levee, interchannel and outer fan fringe deposits and are composed of fine grained sands or silt and graded beds

- *Mass transport complex* (Weimer, 1989): generally a seismic facies description they are hummocky and mounded reflections with poor to fair continuity; sediments that occur at the base of sequences and are overlain and or onlapped by channel and levee sediments. They commonly overlie and erosional base upfan, becoming mounded downfan and are externally mounded in shape and pinch out laterally

- *Slides* (Jackson, 1997): a mass movement or decent from failure of earth

- *Condensed sections* (Loutit et. al., 1988): thin marine stratigraphic units that consist of pelagic to hemipelagic sediments characterized by very slow sedimentation rates. They are areally extensive at the time of maximum regional transgression of the shoreline

Well Logs in Ursa Basin

The Ursa well is a vertical well at the intersection of two seismic sections in the Mars-Ursa Intraslope basin. A map of the basin with the well and 2-d seismic line locations can be seen in Figure 3. The Ursa #1 well was correlated to logs previously interpreted by Lawrence Meckel et. al (2002) and Fred Hilterman (2001). On each well, Figure 4 shows gamma logs on the left and resistivity logs on the right. Resistivity values were used to help interpret fluid saturation, which is distinguished by color. Red represents oil; green represents gas and blue brine. It was assumed that Meckel et al also had additional production data to aid in the interpretation but no details were published. The gamma signature distinguishes sand from shale. Shape of the gamma signature helps to identify facies type and will be discussed in further detail. Reservoir intervals were interpreted based on depositional context as well as fluid saturation. The depositional history shown in Figure 4 helped with interpretation of reservoir intervals. The Ursa #1 well was merged with the log interpretation of Mars, Princess, and Ursa A4 by Meckel et al. The reservoir intervals show good correlation and continuity in expected stratigraphic intervals. Four to five facies have been identified in this basin and are commonly found Intraslope basin settings. The identified facies including amalgamated channels, non-amalgamated channels, condensed section and slope debris flow facies. The most continuous reservoir intervals in the Ursa Intraslope basin are the sheets sands, which are connected between well logs on Figure 1 with magenta lines. The reservoir intervals that were interpreted were Carmine sands, Magenta sands and upper Yellow sands. Identified amalgamated sheet sands are the Upper and above magenta reservoir intervals which are gas and oil saturated respectively. Note that the Upper and Lower reservoir intervals in table 1 were not shown on the Ursa basin well logs in Figure 1.

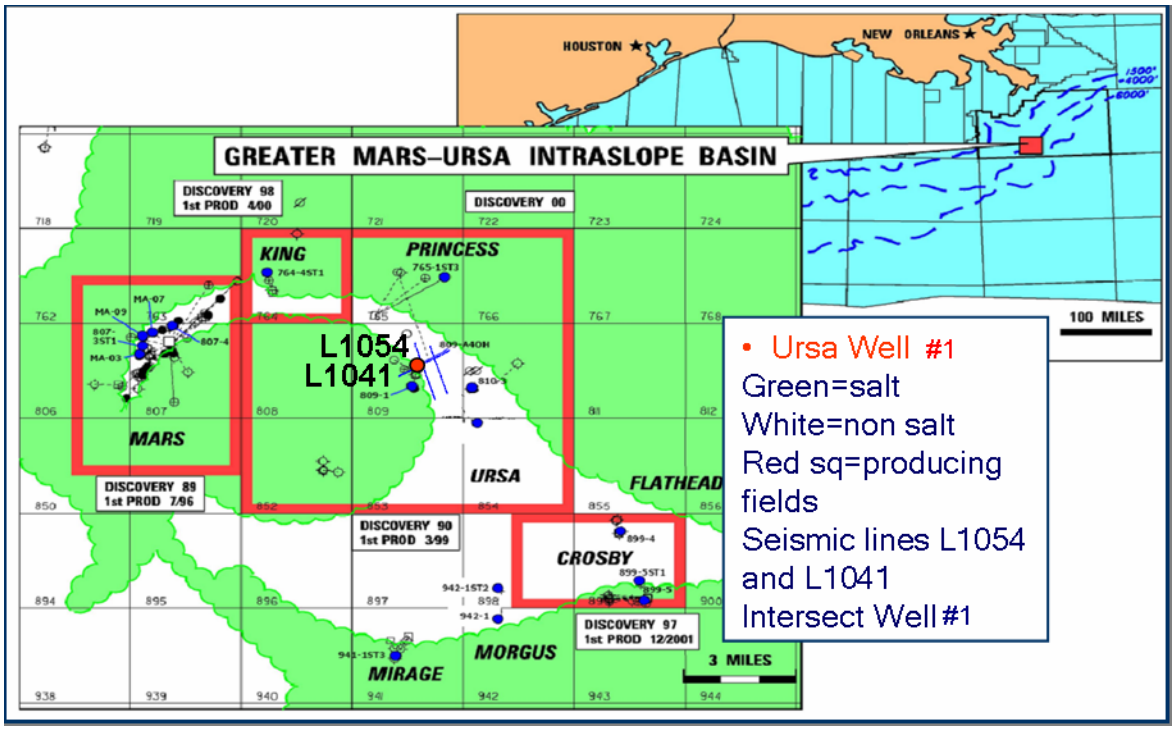

Figure 3: Map of Mars-Ursa Intraslope basin green areas show salt structures, white are non salt structures, red squares show producing field boundaries and red dot shows the Ursa well #1 which intersects with seismic lines 1054 and 1041 (Adapted from Meckel et.al., 2002)

Table 1 shows the various reservoir intervals and their interpreted properties based o work by Meckel et al (2002) and Hilterman (2001). These properties included fluid saturation, pay thickness, Pressure, Stratigraphic Facies, Identified tops and bottoms of logs, average compressional velocity, average estimated shear velocity, average density for each reservoir interval, and the time that the events occurs after applying the checkshot correction on the well log. It should be noted that the shear wave velocities were estimated shear wave which was estimated using the Greenberg-Castagna relations and the log was hung on Hiltermans interpretation of the oil zone which is a prominent feature on the well log. Average reservoir velocities and densities were estimated using histograms and cumulative frequencies to determine the dominant velocity in the individual reservoir intervals and the cap rock/shales above the intervals. Examples of these can be seen in figures 6-9 and additional results can be seen in Appendix A. Before well log analysis, shear wave was estimated and fluid substitution was performed on the well and also AVO/AVA analysis was preformed on the well log data. These will be discussed in following sections.

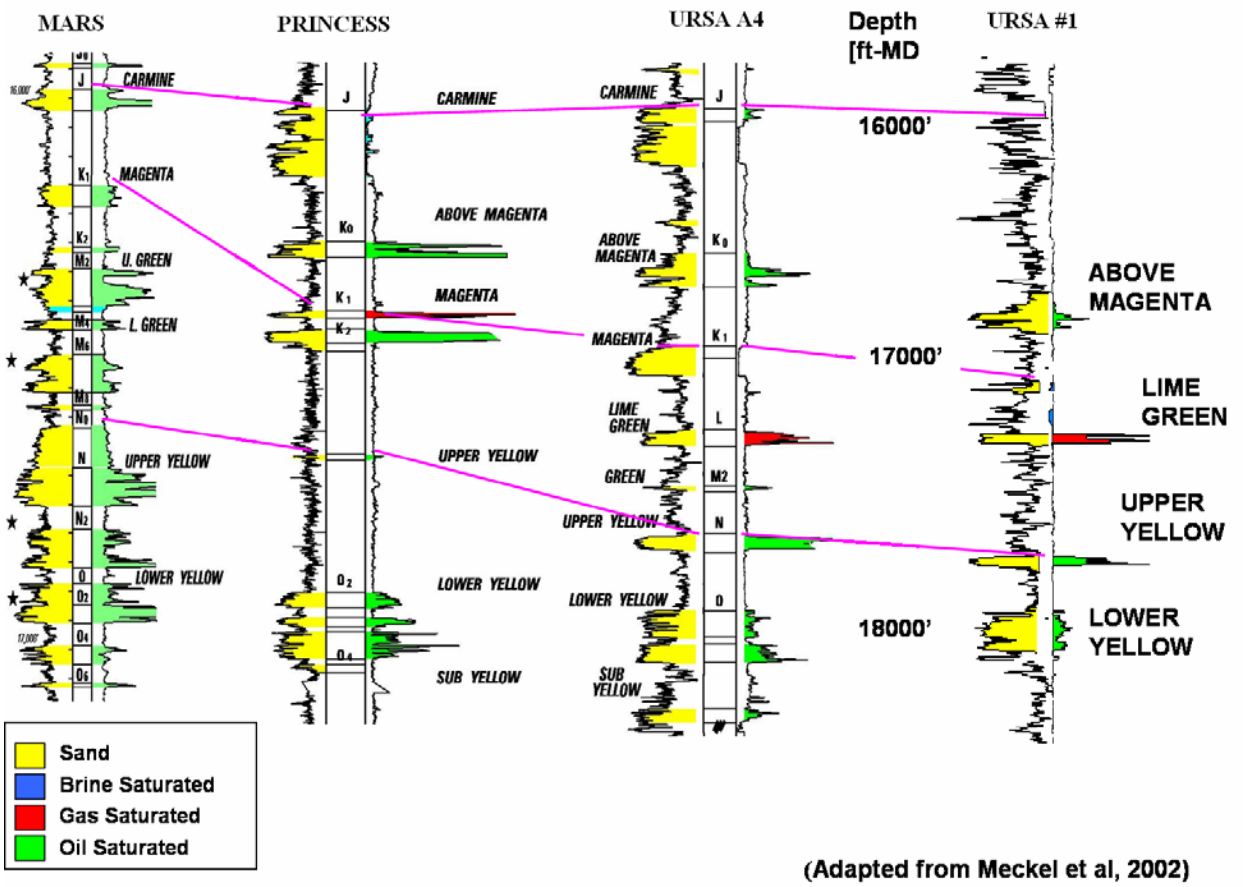

Figure 4. Wells in Ursa Intraslope Basin showing major reservoir intervals. Pink lines connect sheet sands through the basin. Each well has a gamma (right) and resistivity log (left associated with it that was used to interpret sand vs. shale presence and fluid saturation respectively

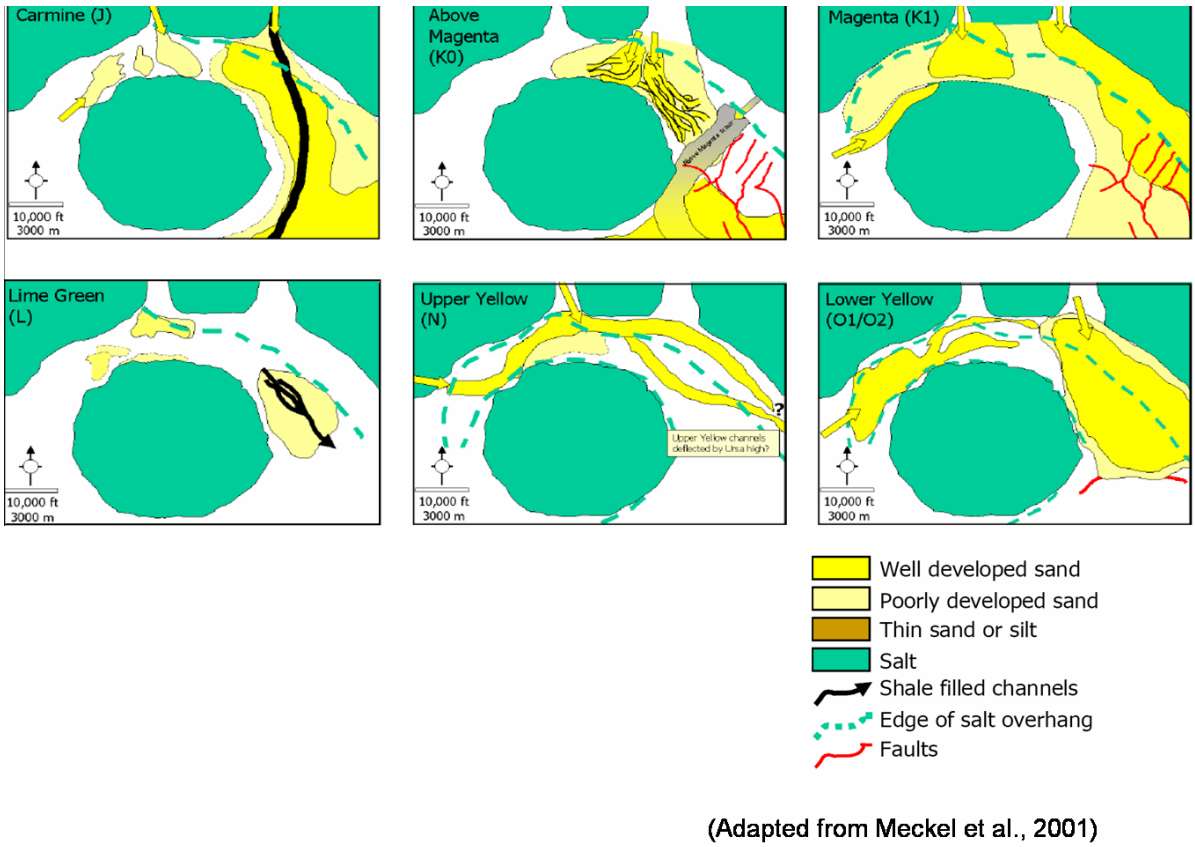

Figure 5. Ursa Basin depositional history for 6 different reservoir intervals. Carmine, Above Magenta, Magenta, Lime green, upper yellow, Lower Yellow

Mars-Ursa Intraslope Basin Reservoir Intervals in Ursa #1 Well								
RESERVOIR	FLUID THICKNESS [Ft] (Hilterman, 01)	Pressure [psi] (Meckel et al, 02)	STRATIGRAPHIC INTERP 4th order (Meckel et al, 02)	TOPS and Bottoms in Well#1 [MD-FT]	Vp avg [m/s]	Vs avg [m/s	Rho avg [g/cc]	Time [ms]
Upper (12000')	OIL 37	N/A	Thin beds	11940-11980	2597.26	1151.55	2.26	4008-4018
Lower (12460')	GAS 19	N/A	Sheet Sand	12400-12421	2308.72	1348.53	2.23	4110-4131
CARMINE	OIL	2200	Sheet Sand	~16000	--	--	--	--
ABOVE MAGENTA	OIL 55	2200	Amalgamated channel system	16760-16866	2840.06	1577.44	2.28	5231-5235
MAGENTA	BRINE	2200	Sheet Sand	17054-17106	3164.25	1684.86	2.38	5272-5282
BELOW MAGENTA	BRINE	2200	Sheet Sand	17169-17225	3197	1398	2.37	5294-5304
LIME GREEN	GAS 38	2200-3000	Non amalgamated channel?	17250-17302	2664.8	1480.91	2.19	5309-5321
UPPER YELLOW	OIL 39	3900	Non amalgamted channel	17749-17820	3042.73	1622.24	2.30	5409-5423
LOWER YELLOW	OIL 167	3900	Sheet sand	17976-18182	2965.7	1595.35	2.26	5454-5496

Table 2. Mars Ursa Intraslope basin reservoir properties

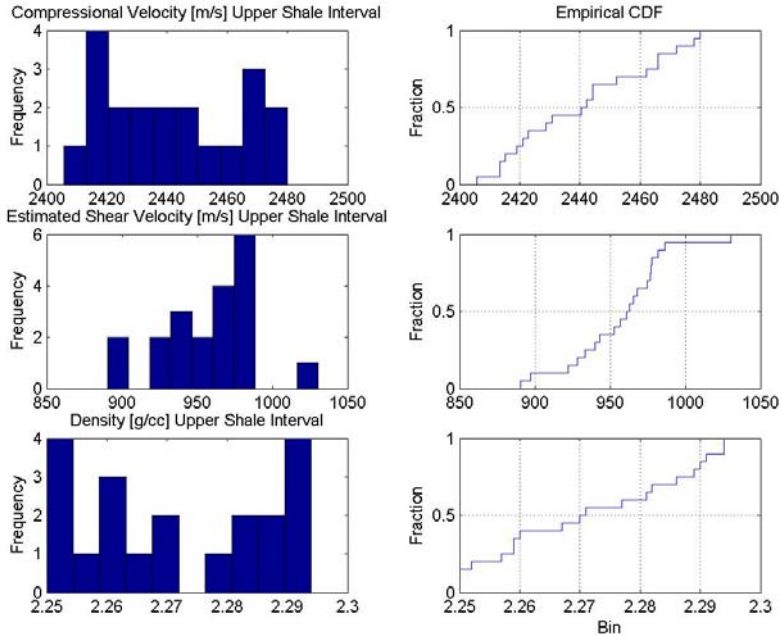

Figure 6. Histograms and empirical CDF curves for VP, estimated Vs and Density for the Upper Shale Interval

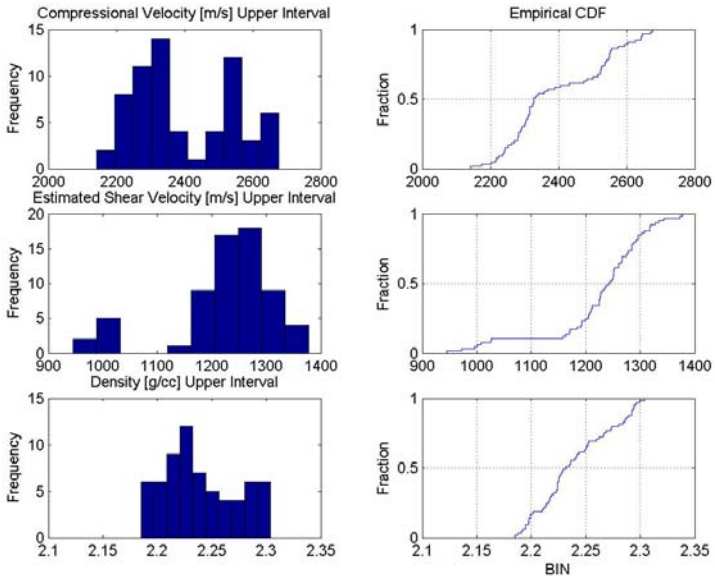

Figure 7. Histograms and empirical CDF curves for VP, estimated Vs and Density for the Upper Reservoir interval

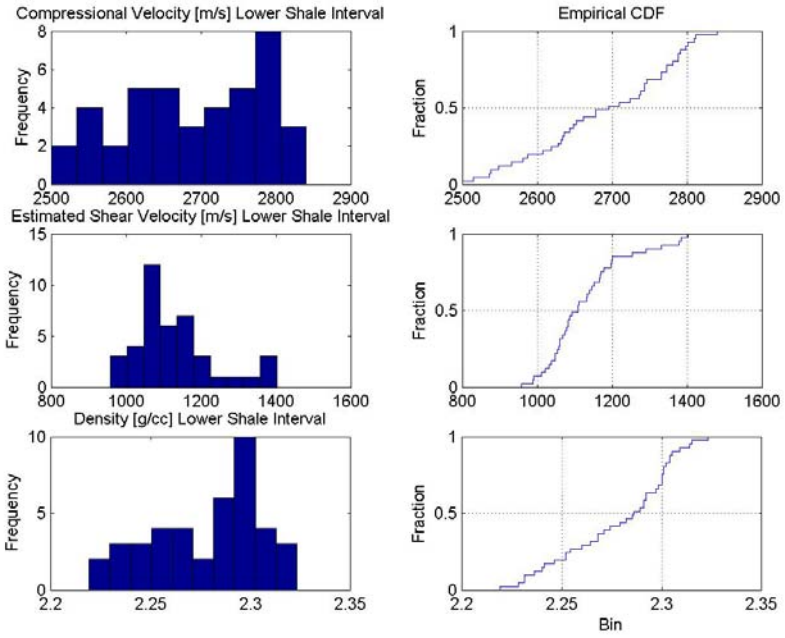

Figure 8. Histograms and empirical CDF curves for VP, estimated Vs and Density for the Lower Shale

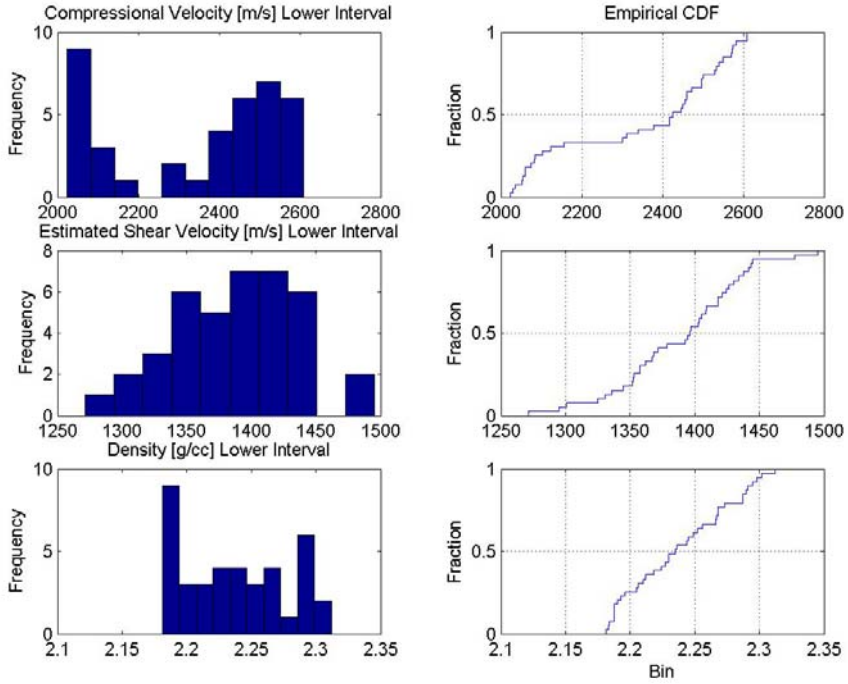

Figure 9. Histograms and empirical CDF curves for VP, estimated Vs and Density for the Lower Reservoir interval

Outcrop expressions of Deepwater facies

Expressions of deepwater facies in outcrop can be correlated to the well log and seismic signature. Sheet sands, condensed sections, amalgamated and non-amalgamated channels can be seen in figures 10-13. Sheet sands are generally widely continuous over large areas and can range from 3-25 km in lateral extent and hundreds of feet in vertical extent. (Weimer and Slatt, 2003) Sheet sands are easily correlatable between wells and are parallel and laterally continuous in seismic expressions, they tend to be bounded by condensed section. Comparison of sheet sand in outcrop is made to seismic expression and well log expression in figure 10. Note that the scale of sheet sands in outcrop is not directly correlatable to the seismic. The well log expression of sheet sands is blocky or bell shaped and they tend to have flat bottoms.

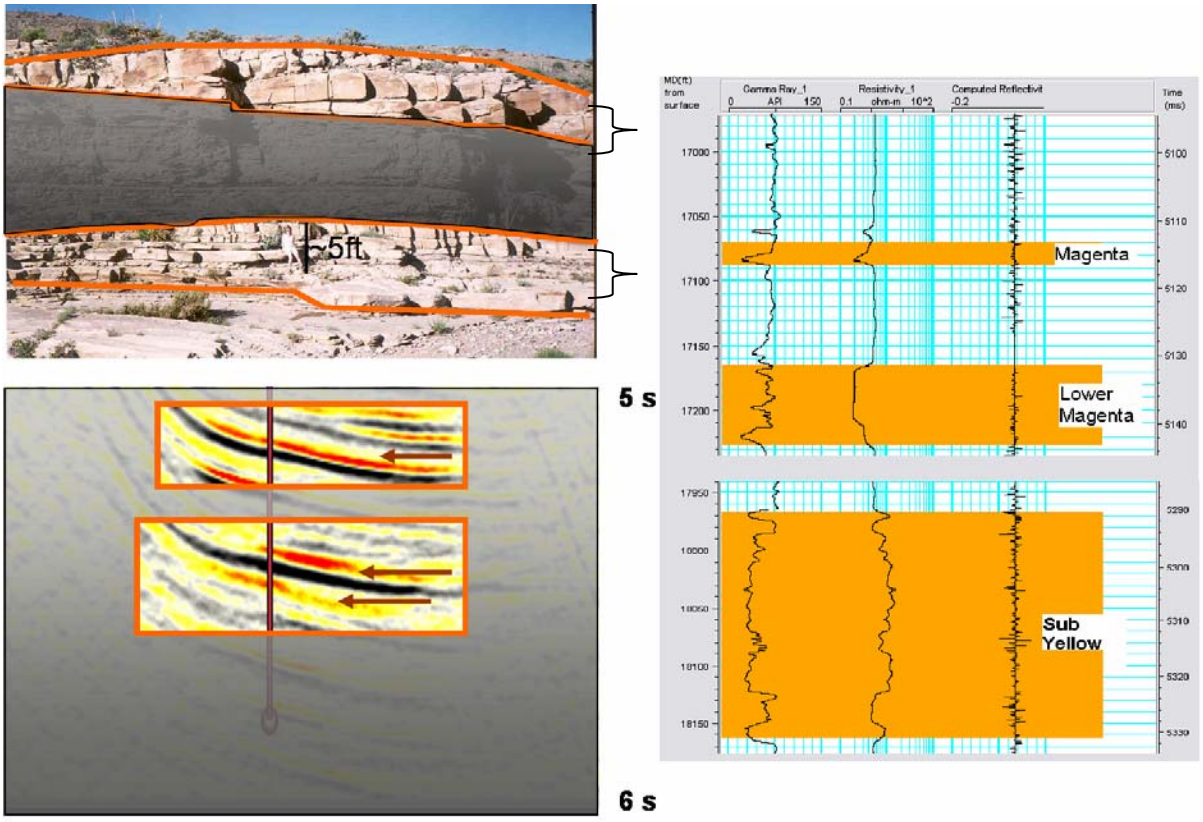

Figure 10. Sheet sand expression in outcrop, seismic and wireline response. Note scale of outcrop is approximately 1/4 of the seismic scale.Outlined area shows sheet sand structures in outcrop and seismic. Highlighted area on logs show sheet sand sin log expression

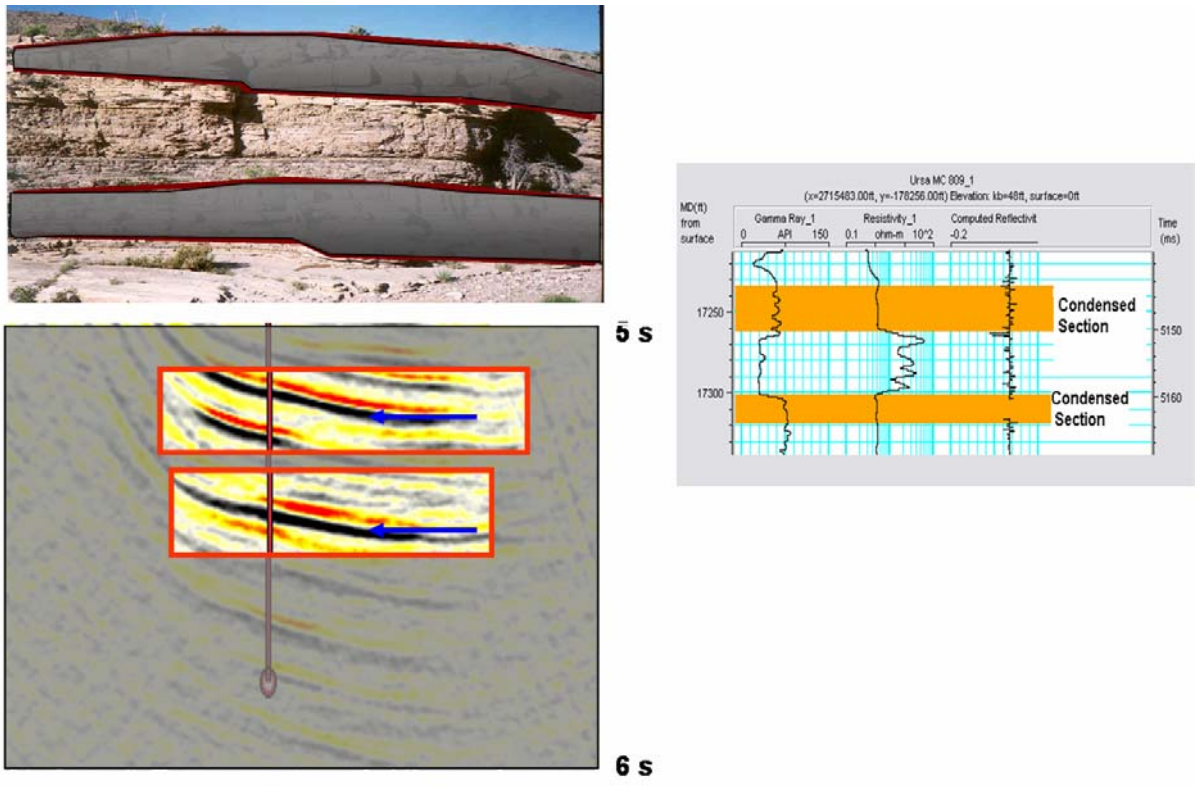

Figure 11. Condensed section expression in outcrop, seismic and wireline response. Note scale of outcrop is ~1/4 of the seismic expression

Condensed sections are also highly continuous over large areas. Condensed sections are usually easy to identify because the occur as “hard” seismic events and are associated with high gamma reading in the well log response. Comparison of a condensed section in outcrop is made to the seismic expression and well log expression in Figure 11. Note that the scale of the condensed section in outcrop is not directly correlatable to the seismic seismic.

Channel sands can be amalgamated or non- amalgamated and generally are expressed as discontinuous sub-parallel reflections in seismic with low correlatability between wells. Channels can range to be about 3 km wide and can be up to 100 m thick in vertical expression. In seismic data channels are usually observed as composites of numerous smaller channel cuts. Figure 12 shows a good example of the expression of a non amalgamated channel in outcrop. In seismic we can see the limited extent of the channel

feature and the block expression on the well log. Another common deepwater facies that is associated with channels are thin bed levee deposits. These features can range from .8-8 km horizontally and are usually less than 30 m vertically. Thin bed levee deposits have potential to be significant reservoirs. Usually the display as gull wing structure in seismic and have sub-parallel to poor continuity. The log expression of these features is usually serrate to fining upward and correlatability is moderate to poor. The lithology is usually thin bedded and less than 8 cm thick bedding. (Slatt & Weimer, 2003) The log and seismic expression of thin bed levee deposits can be seen in Figure 13. Table 2 presents a summary of all of the deep water facies and their expression in well log, core and seismic.

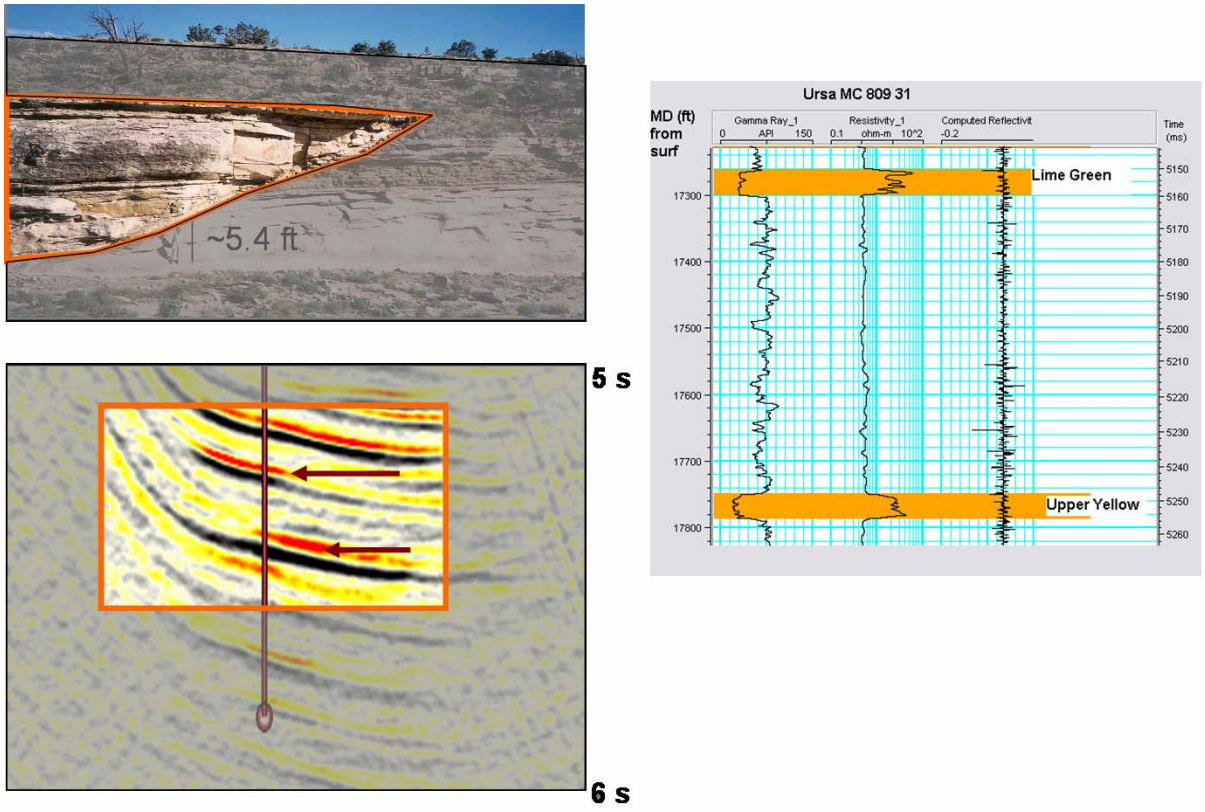

Figure 12. Non amalgamated channel in outcrop on seismic and wireline response

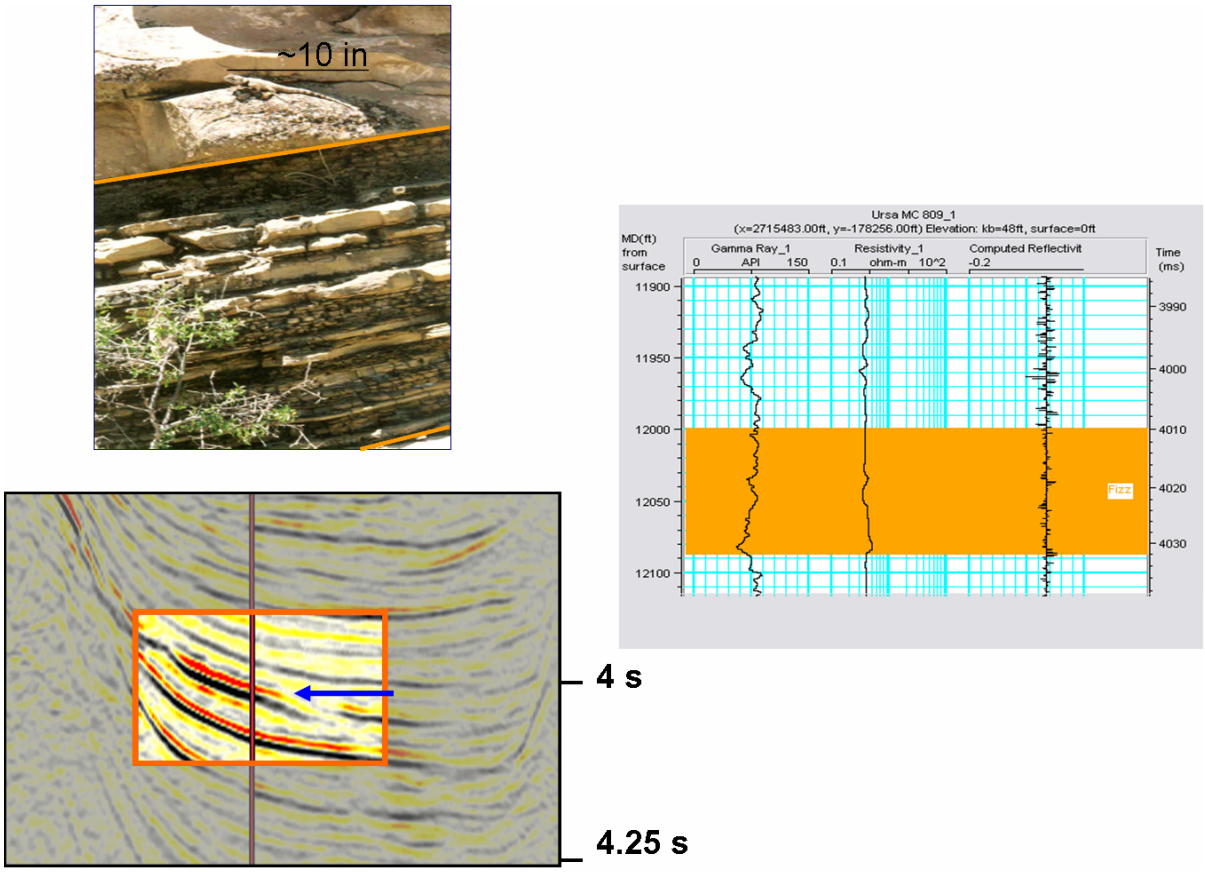

Figure 13.Thin beds in outcrop, seismic and wireline response. Note scale of outcrop is approximately 1/4 of the seismic scale. Outlined area shows sheet sand structures in outcrop and seismic. Highlighted area on logs show sheet sand sin log expression

	Geologic	Well log	Seismic
Sheet Sand	Good lateral continuity, tabular geometry, fairly heterogeneous	Single to multiple units Blocky and bell shaped with flat bottoms Highly correlatability	Wedge shape and usually expressed as a single seismic event
Non Amalgamated channel	Thick to thin bedded, internally homogeneous	Blocky and bell shaped Poor correlatability	Shingled Seismic Sub parallel
Amalgamated Channel	Limited sand bodies	Blocky and rounded or serrate and change over distance	Shingled seismic geometry Sub parallel
Slope and Debris Flow/Mudstone	Soft sediment deformed , planar laminated silty claystone	High gamma Poor correlatability	Chaotic discontinuous
Thin Bed levees	Thinly bedded sands and silts <4" beds	Thinly bedded /laminated sands and silts fining uppward Poor correlatability	"gull wing" to sub parallel
Condensed Section	Composed of mud and organics represent long time intervals maximum water depths separate sheet sands below from channelized surfaces	High gamma values Highly correlatability	Occur at base of sheet sands; acoustically "hard" seismic events Continuous and high amplitude

Table 3. Summary of deepwater facies in outcrop, wireline and seismic

Petrophysical Modeling

Petrophysical modeling was preformed on the Ursa log to examine the AVO response of individual reservoir intervals. Hilterman (2001) published an approximation similar to Shuey's (1986) approximation of the Zoeppritz equations to get a better idea of the relationship of lithostratigraphic and chronostratigraphic events.

$$RC(\theta) \sim NI \cos^2(\theta) + PR \sin^2(\theta) \qquad \text{Eq. 1}$$

The reflection calculated as a function of angle of offset for the normal incidence reflectivity (NI) which relates velocity and density and Poisson reflectivity (PR) which relates elastic properties of the rocks which are both functions of lithology. This approximation was used to evaluate the AVO response for the reservoir intervals in the Ursa log. For each reservoir the average velocities and densities for the cap rock and reservoir interval were used for the calculations. These were modified using results from histograms and CDF's presented earlier in the paper. Results of these AVO models can

be seen in figures 14-17. All results are consistent with the seismic data in the sense that the bright spots observed in seismic data also show class III AVO response. Response's for sheet sands, amalgamated and non amalgamated channels are grouped together in order to identify significant trends for specific facies.

Seismic Facies Estimations

Brine substitution was performed on the Ursa #1 well in each of the reservoir intervals using Hampson Russell software. The results of each fluid substitution for individual reservoir intervals was then merged with the original well log. Each facies was then grouped with similar facies and velocity and density for each of those facies were averaged to see if any one facies would stand out. The plots of these various distributions can be seen in figures 18-20. It seems that the velocities and densities from particular facies overlap to the point that they cannot be easily distinguished from each other but there are some telling characteristics of the statistical results that may aid in facies interpretation. For example, for velocities and densities of sheet sands and condensed section are normally distributed which is expected due to their highly continuous and internally homogeneous character. Channels and thin beds tend to have bimodal distributions indicating that there are two lithologies present.

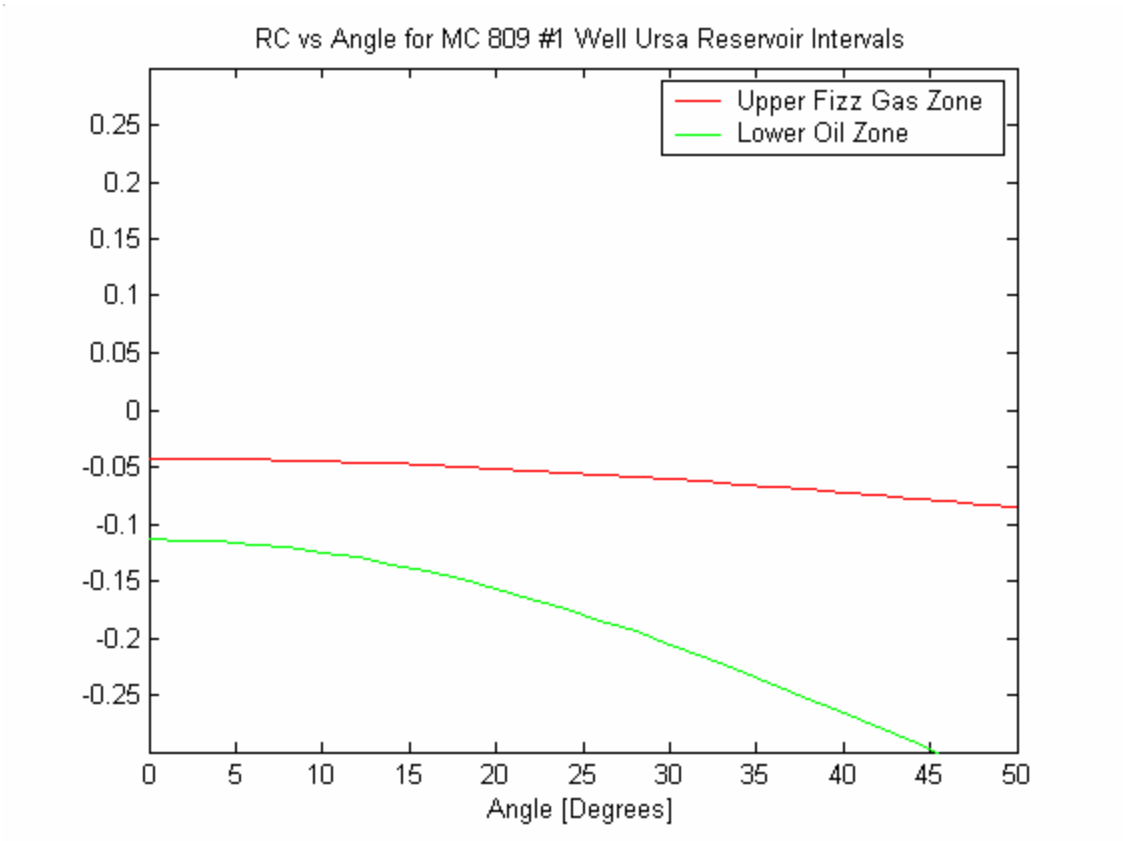

Figure 14. AVO model of upper fizz gas zone and lower oil zone (upper shale 11980-12000 upper 12000-12100 lower shale 12381-12400 lower 12407-12418)

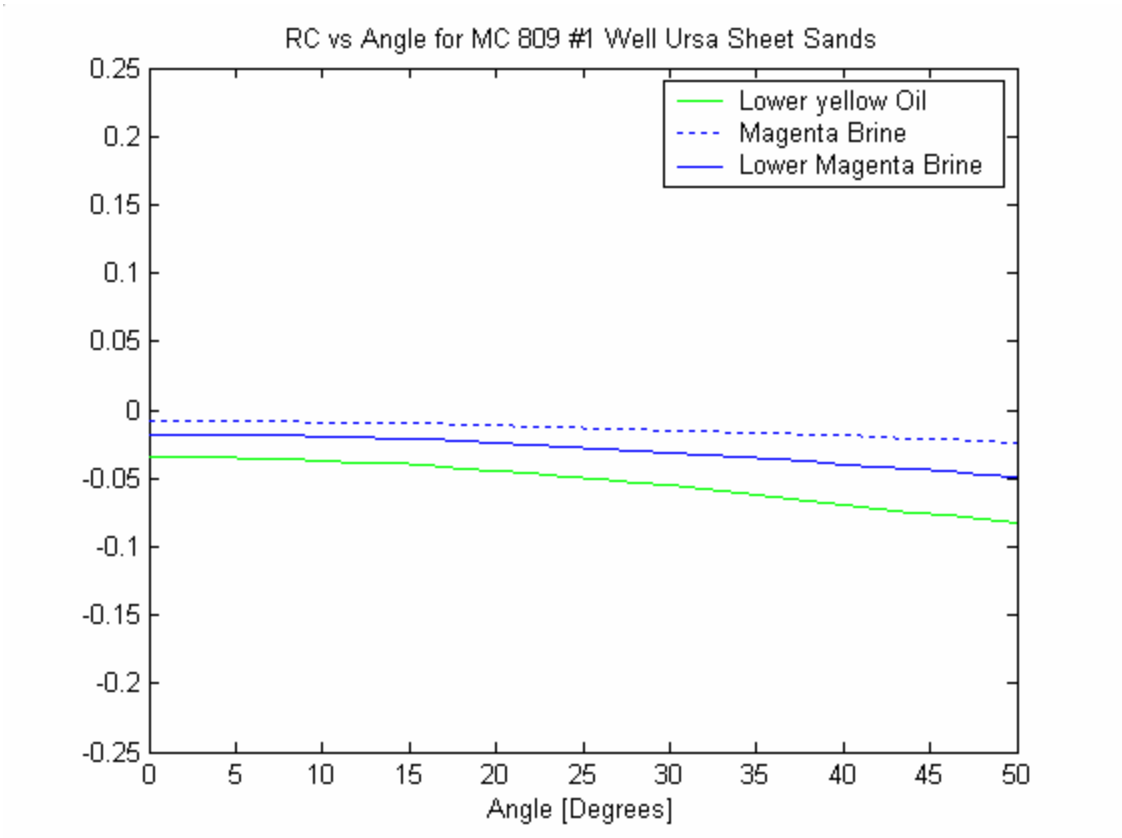

Figure 15. AVO response for sheet sands in Ursa Log #1

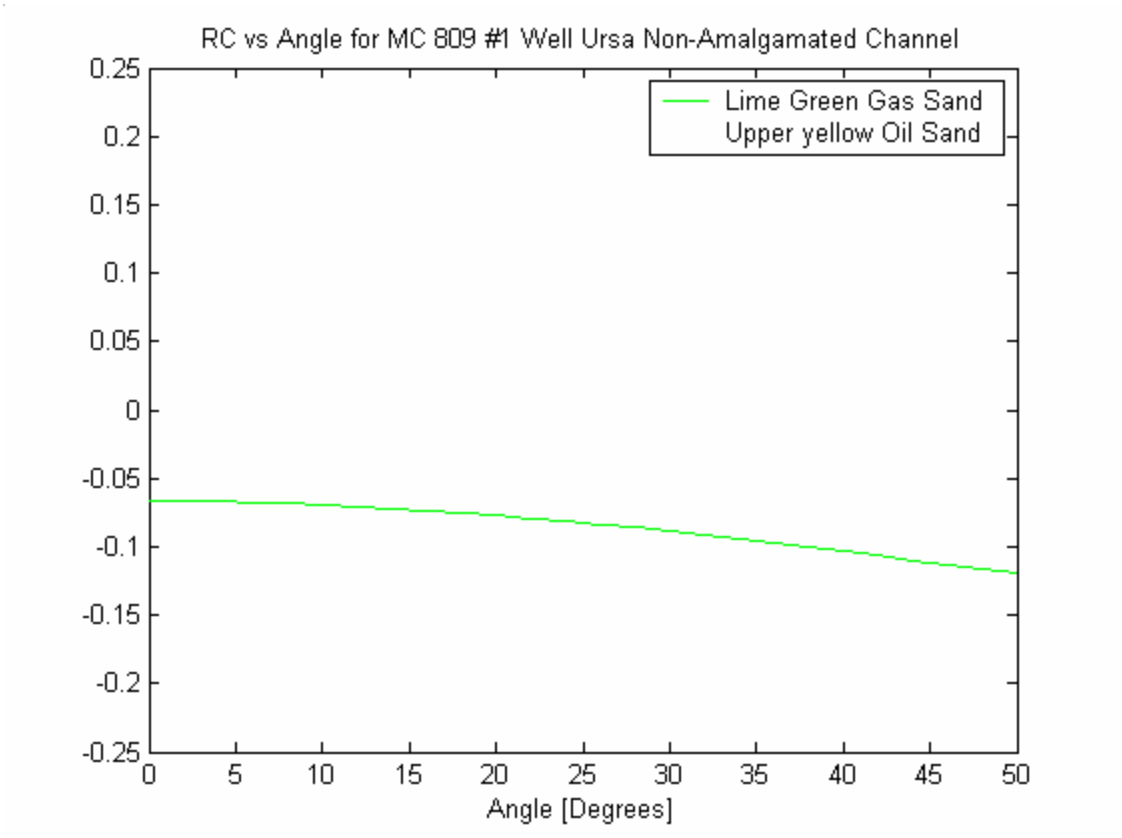

Figure 16. AVO response for amalgamated sheet sand in Ursa #1 log

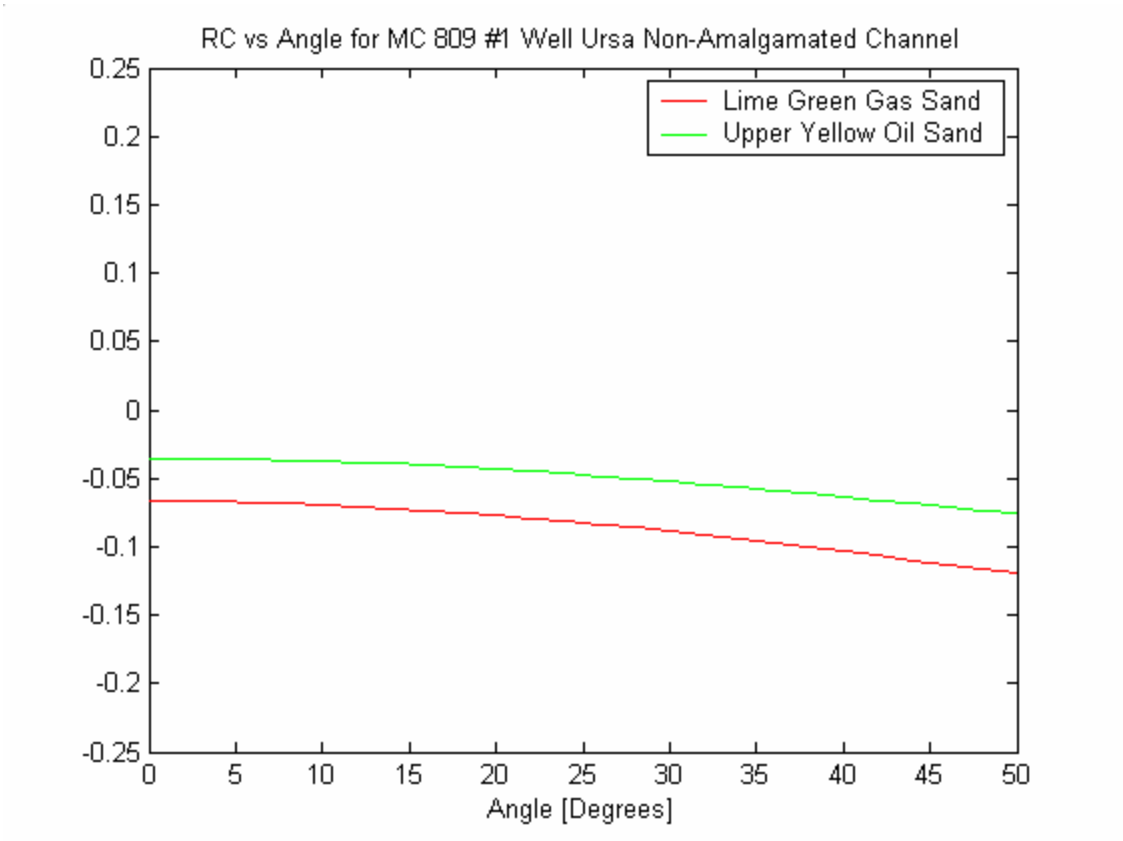

Figure 17. AVO response for non amalgamated channel sands

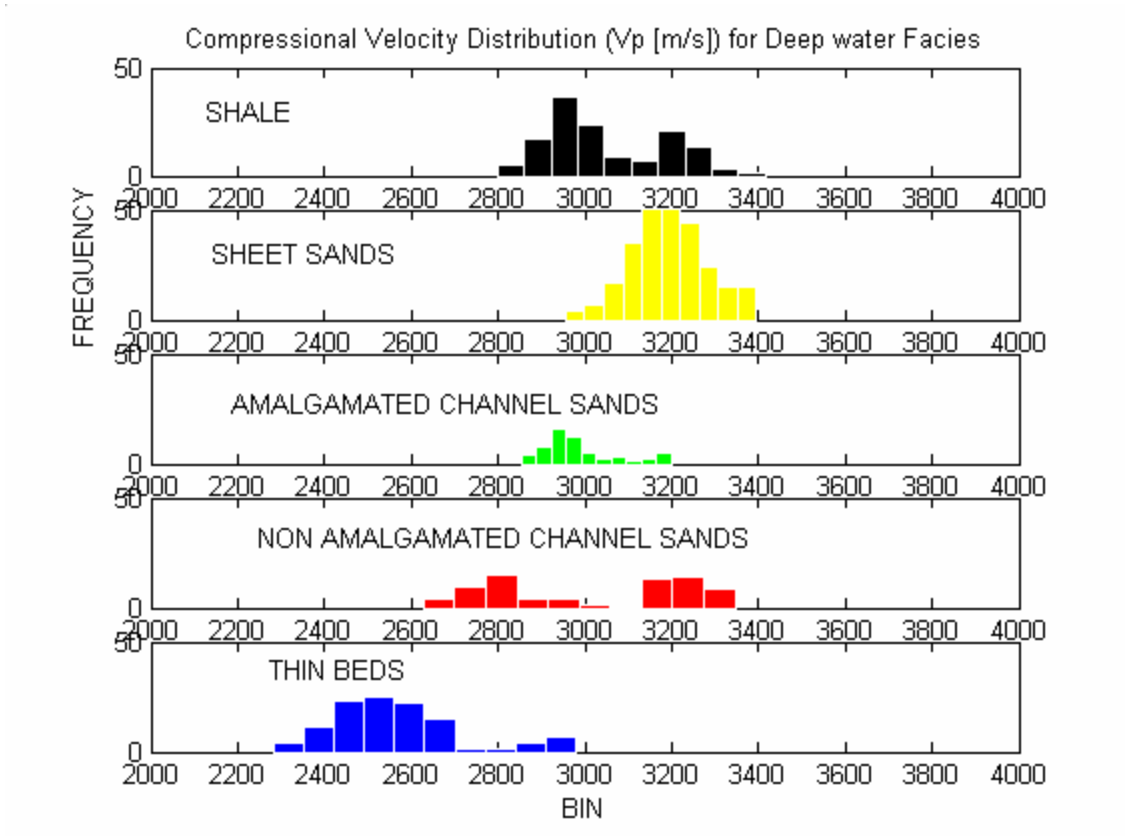

Figure 18. Compressional velocity distributions for deep water facies in Ursa well #1. Note that bimodal distributions in several facies indicate mixed lithology.

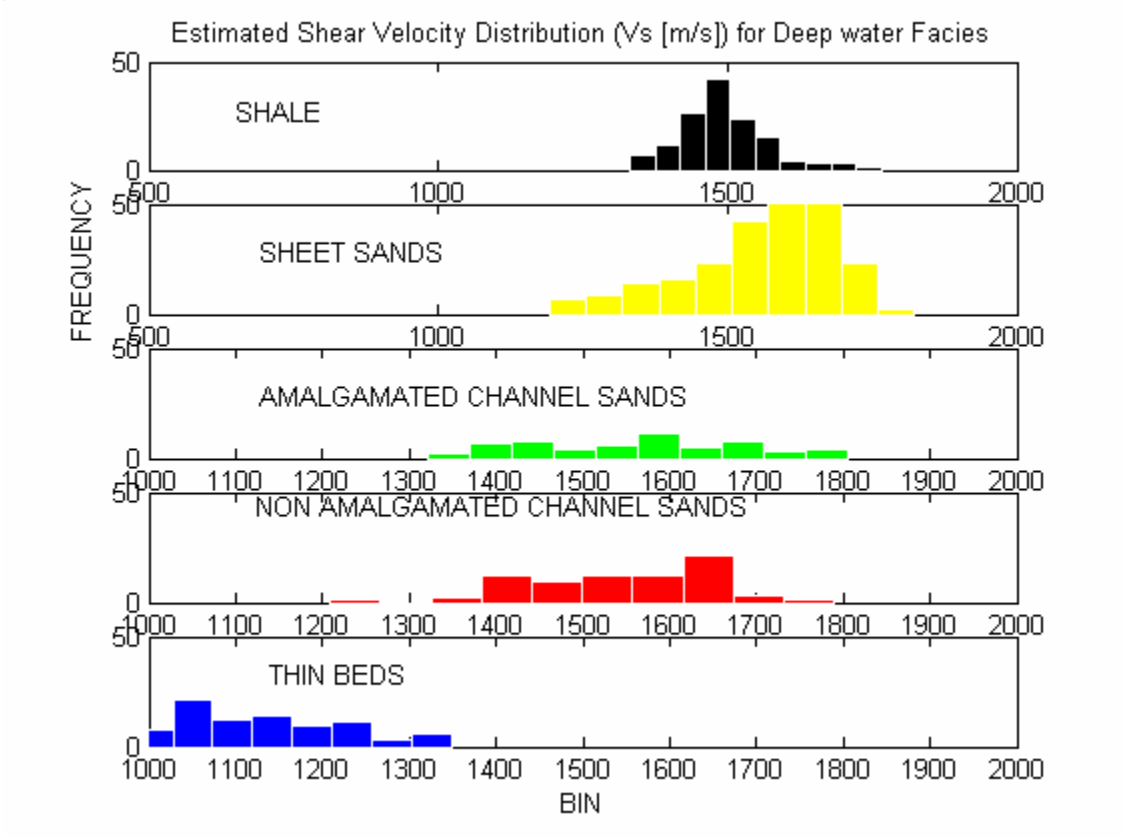

Figure 19. Estimated Shear velocity for deep water facies for Ursa well #1

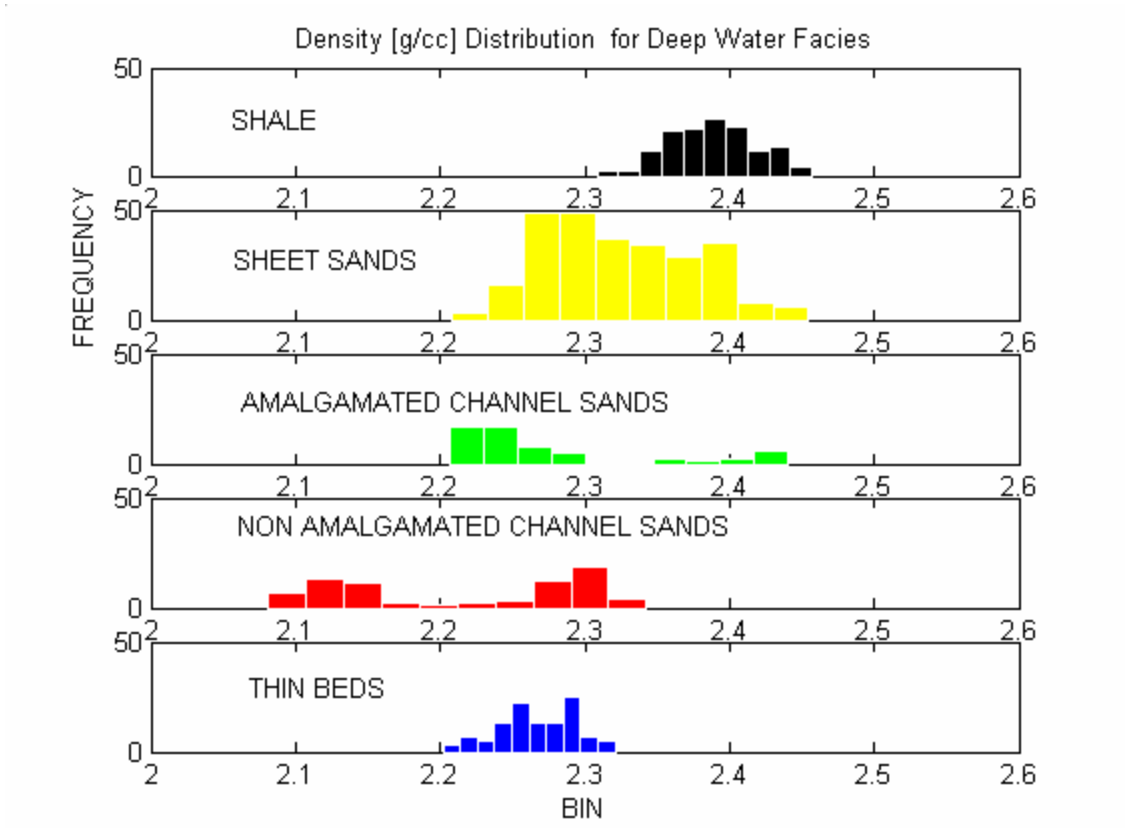

Figure 20. Density distributions for deep water facies in Ursa well #1. Note that bimodal distributions in several facies indicate mixed lithology

Pressure

Pressures obtained from Meckel et. al. (2002) illustrates the function of key reservoir features. In figure 21 it can be seen that there are at least three major changes in the background velocity trend that may be attributed to pressure. The trend of overpressure is plotted as a comparison in figure 22. In can be seen that there is an overlap between the Ursa overpressure zone and the velocity trends in figure 22. As stated before these overpressures are controlled by presence of condensed section (shales) and have an impact on the seismic signature as well.

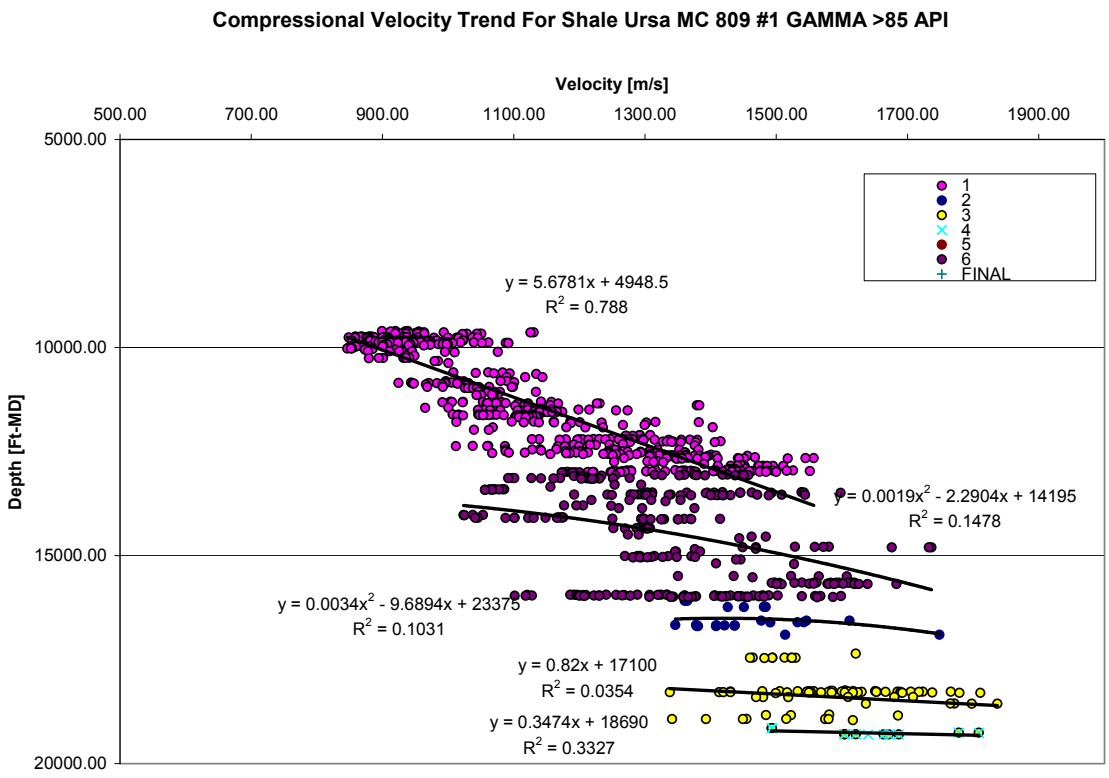

Figure 21. Compressional velocity trend for shale in the Ursa #1 well

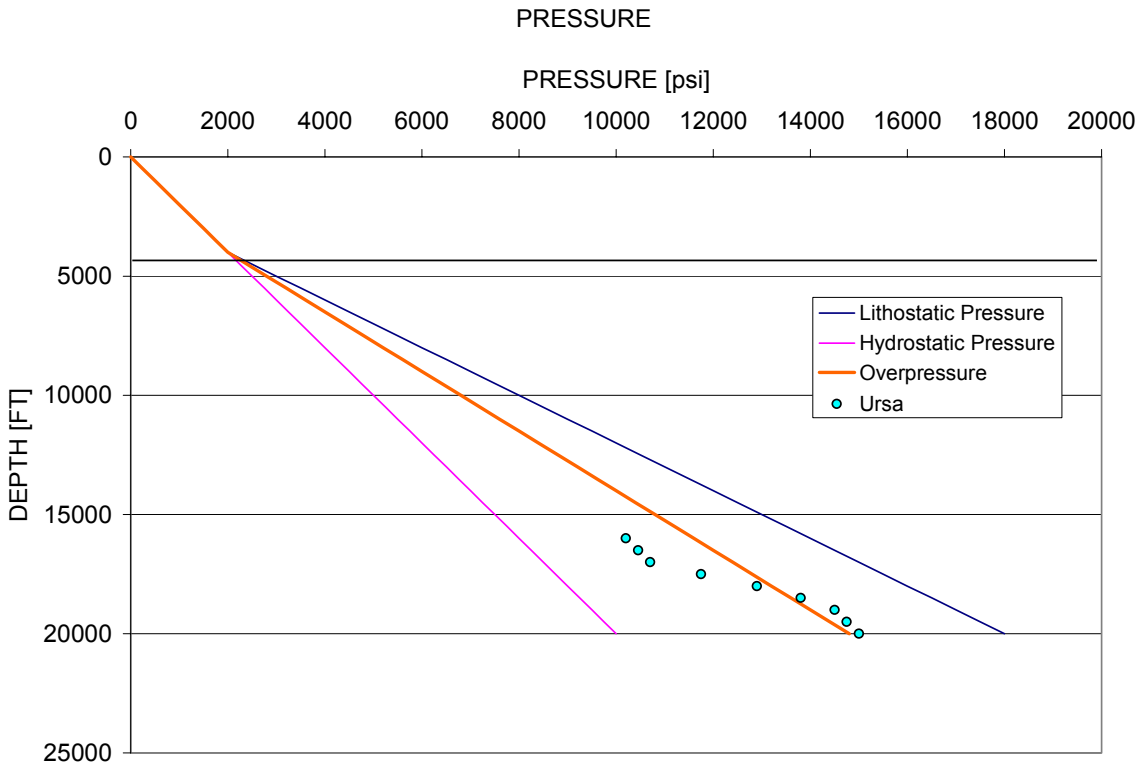

Figure 22. Ursa well overpressure zone

Modeling

I've also attached a zip archive with 4 figures to this e-mail. Two of them are plots of the logs you sent last, including the estimated Vs. Both of these show the original logs in bold lines, on which I've superposed the models used for computing composite reflection coefficients in thinner lines (red for velocity and green for density). It's a little hard to get all the info in one figure, but I think it works ok. You'll see that for both the fizz and the oil model, there is about 30 m of my models exactly reproduce the original logs, and that above and below these sections there are constant velocity values showing the over- and underburden half space velocities I used.

The other pair of figures shows the composite reflection coefficients for the models at 15, 30 and 60 Hz. There are a couple of interesting points in the curves: (1) though results at 15 Hz are fairly similar for both models, the oil reflecting zone increases amplitude more rapidly with frequency (recall especially that a shift at 0 degrees is the same as AVO intercept); but (2) on the other hand, the curves for the oil have nearly the same shape (i.e., AVO gradient) for 15 and 30 Hz, but the fizz reflector changes shape (AVO gradient) even though its intercept doesn't change much. This gives some motivation for looking for clues in frequency dependent AVO. If we're lucky, Seung's data analysis will find something like this.

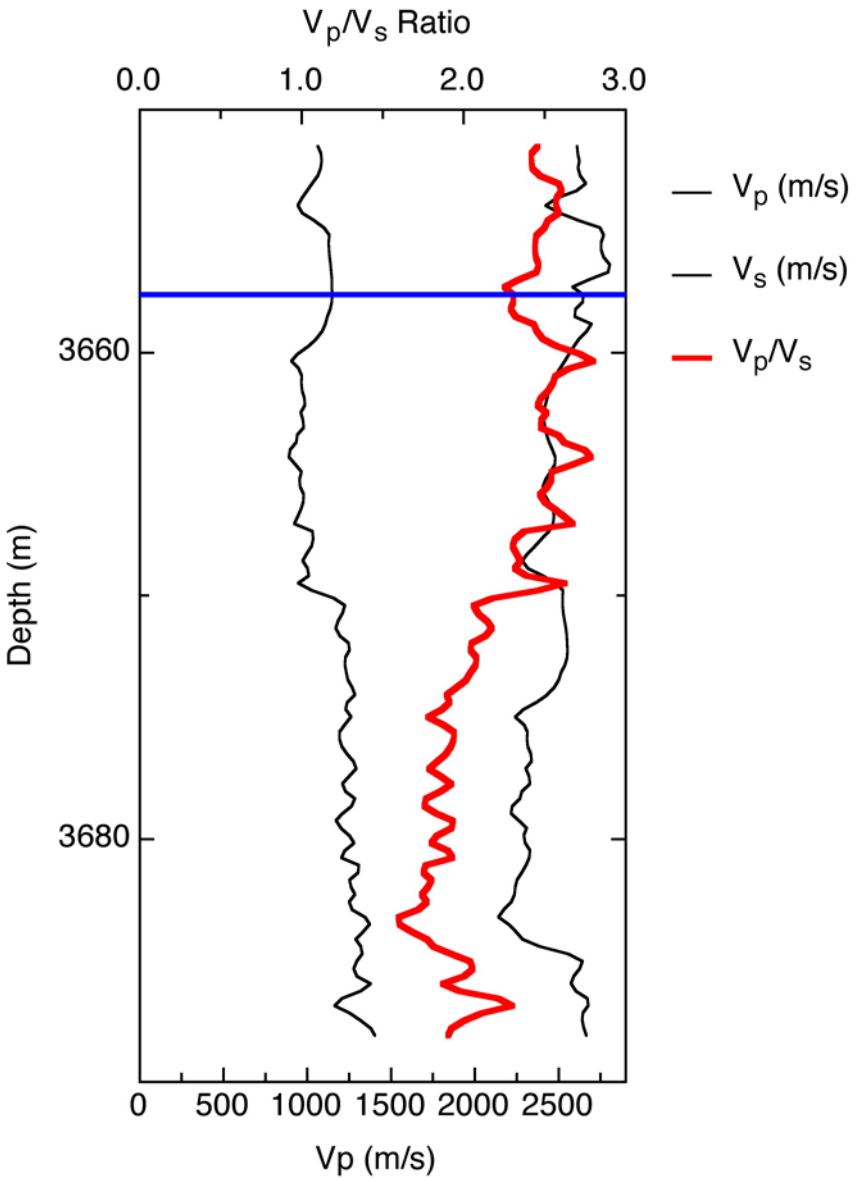

Figure 23. Vp/Vs ratio for Upper fizz gas zone on Ursa well

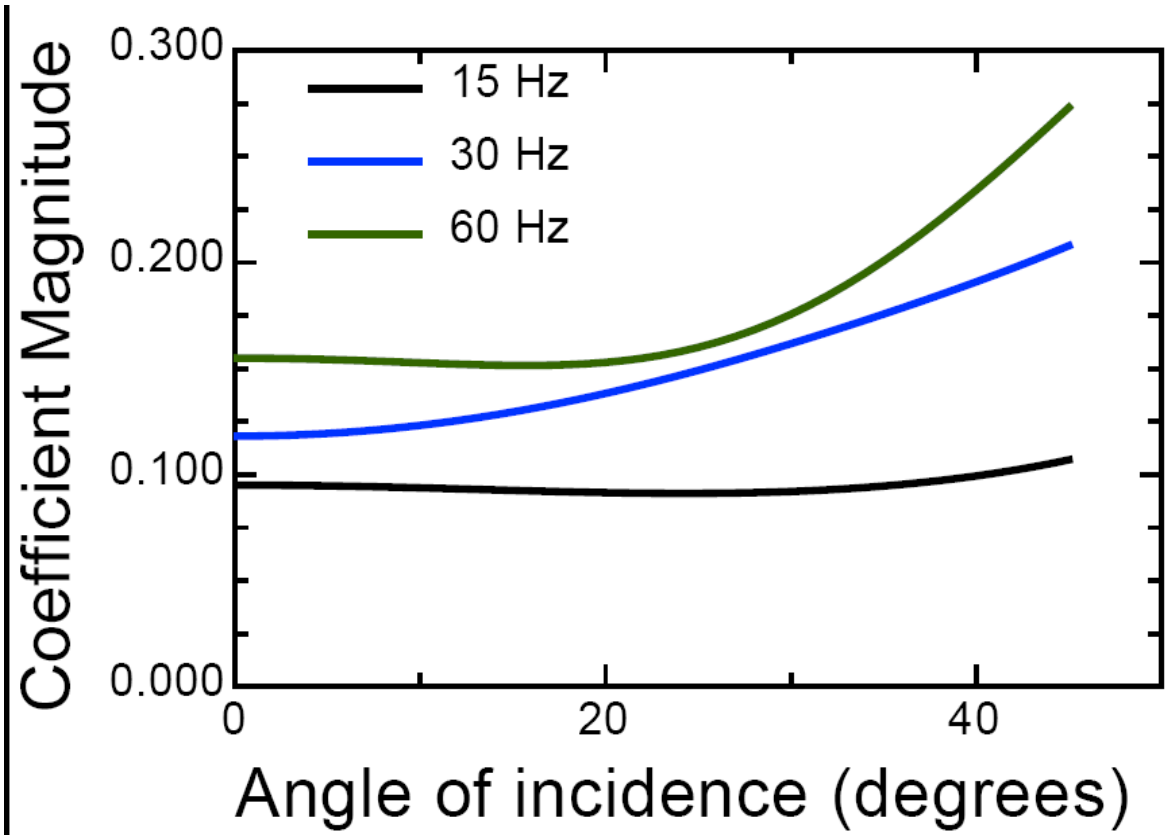

Figure 24.Reflection Coefficient for fizz saturated zone on Ursa #1 well

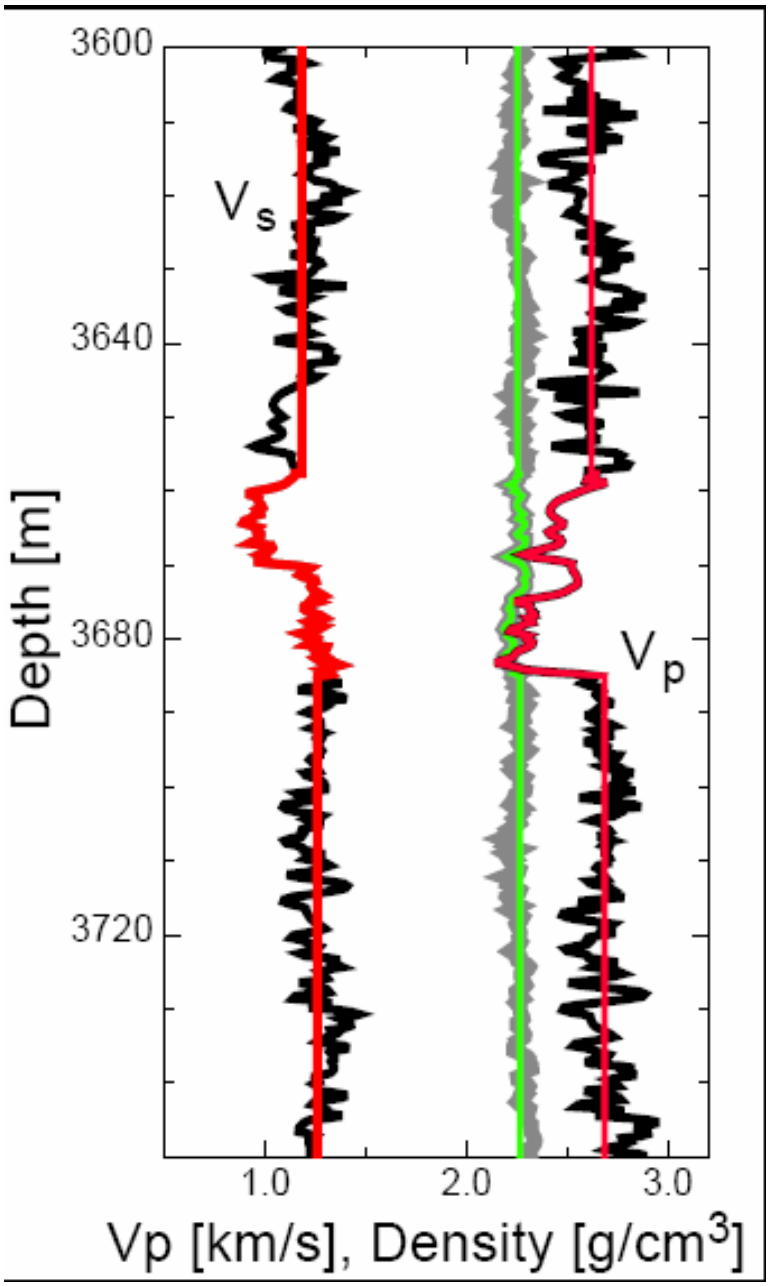

Figure 25. velocity and Density model for fizz saturated zone on Ursa # 1 well

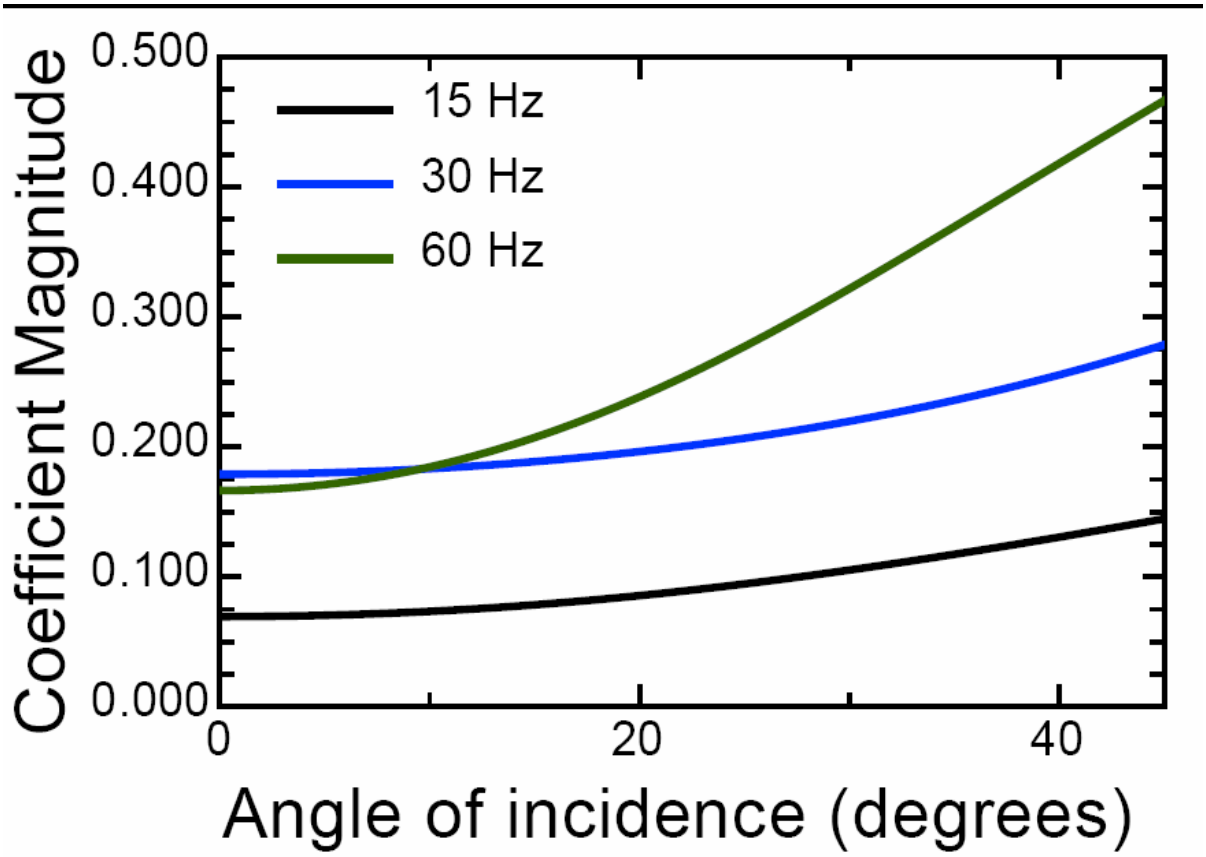

Figure 26. Reflection Coefficient for oil saturated zone on Ursa #1 well

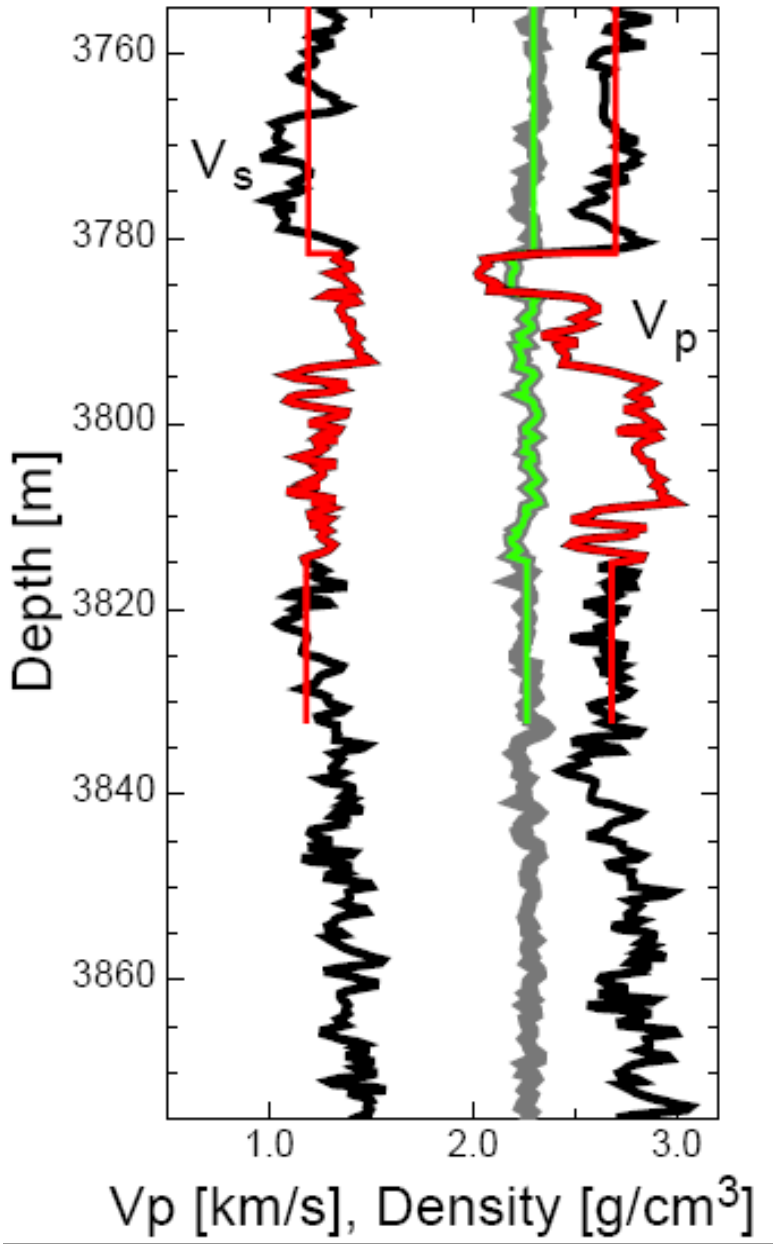

Figure 27. velocity and density model for lower oil saturated zone on ursa #1 well

AVO Analysis using Windowed Fourier Transform

Thin layers can affect seismic amplitude in the same order as sand thickness and reservoir fluids. This causes great uncertainty in using seismic AVO in reservoir characterization. This uncertainty can be reduced greatly by applying a windowed Fourier transform at the target and then analyzing the amplitudes at low frequency. Another benefit of such approach is that the WFT low frequency amplitude is linearly related to reservoir

thickness without the effect of the thin layers, so it can be used to estimate the net sand thickness robustly.

Figure 1(a) compares the tuning curves for two models. One is a three-layer shale/sand/shale wedge model with variable sand thickness, and the second model has two additional thin sands above the sand wedge. The existence of the two thin layers overall decreases the amplitude. At quarter wavelength with amplitude decreases about 33%. The amplitude decreases about 50% for sand thickness greater than half of the wavelength. The decrease of amplitude obviously can confuse the seismic interpretation, especially in the cases where the existence thin layer is also an unknown factor. Figure 1(b) shows the WFT domain amplitudes picked at 10 Hz for both models. The amplitude spectra of the three traces marked by arrows are shown in Figure 2. Since the thin layers affect only the higher frequency, the amplitudes at low frequency shows similar relationship with thickness for both models.

The WFT approach is applied to a field data around King Kong and Lisa Anne wells. King Kong is known to have thin layers around the top of the sand. The existence of such thin layer can reduce seismic amplitude and WFT method is used to reduce such effect. The near and far offset WFT amplitude are cross-plotted in figure 3. It shows a great different between the King Kong field and Lisa Anne prospect after reducing the thin layer effect. This helps to emphase the difference between the two fields.

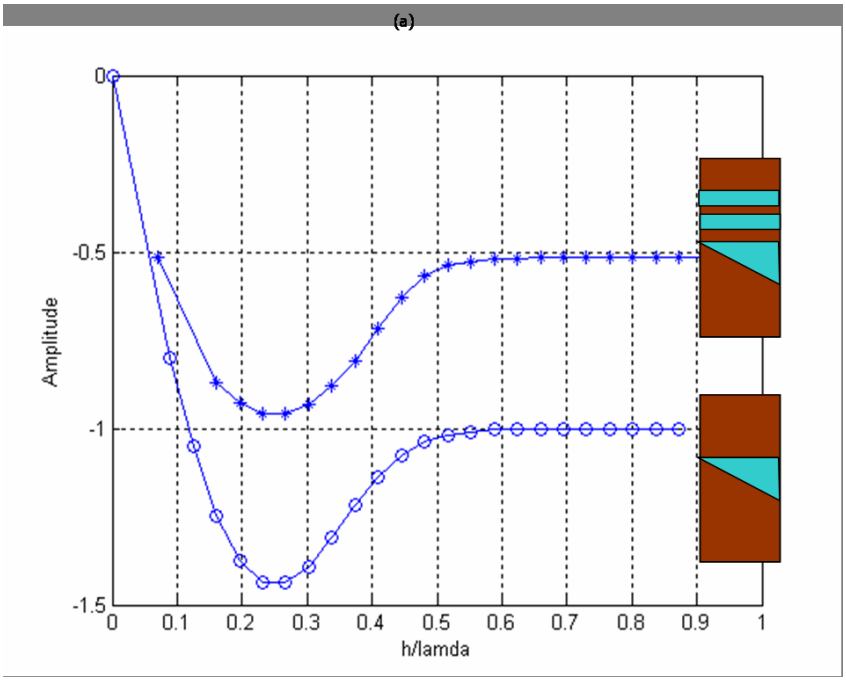

Figure 28. Tuning amplitude curves in time (left) and windowed Fourier transform (right) domains for the models in Figure 25. The two thin sands at the top of the third sand wedge are 2 meters each, about 1/32 of wavelength, λ =64 meters. Horizontal axis is net sand thickness (h) divided by wavelet length. The WFT amplitudes shown on the right

are picked at 10 Hz on the WFT spectra. As examples, the WFT amplitudes points by the three arrows are taken from the WFT spectra in Figure 5 at 10 Hz

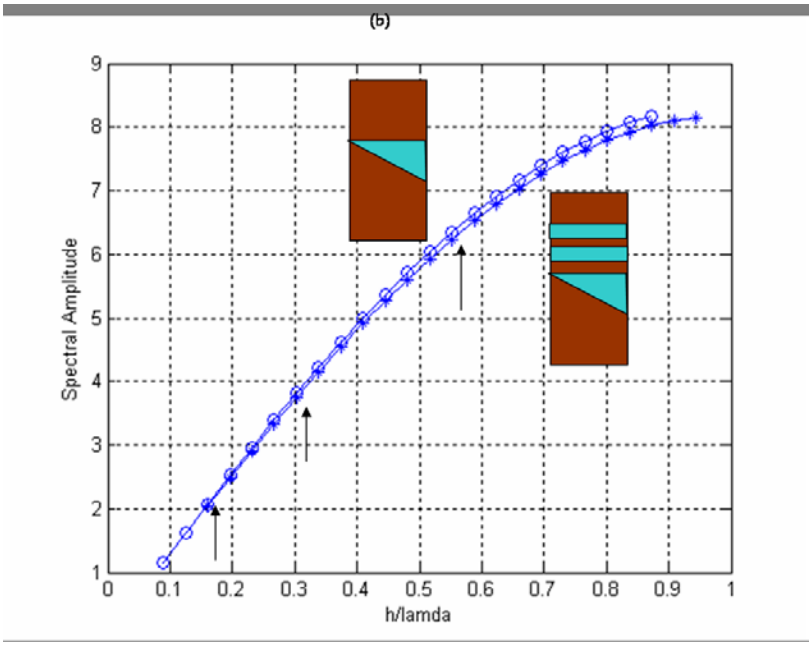

Figure 29. Tuning amplitude curves in time (left) and windowed Fourier transform (right) domains for the models in Figure 25. The two thin sands at the top of the third sand wedge are 2 meters each, about 1/32 of wavelength, λ =64 meters. Horizontal axis is net sand thickness (h) divided by wavelet length. The WFT amplitudes shown on the right are picked at 10 Hz on the WFT spectra. As examples, the WFT amplitudes points by the three arrows are taken from the WFT spectra in Figure 5 at 10 Hz

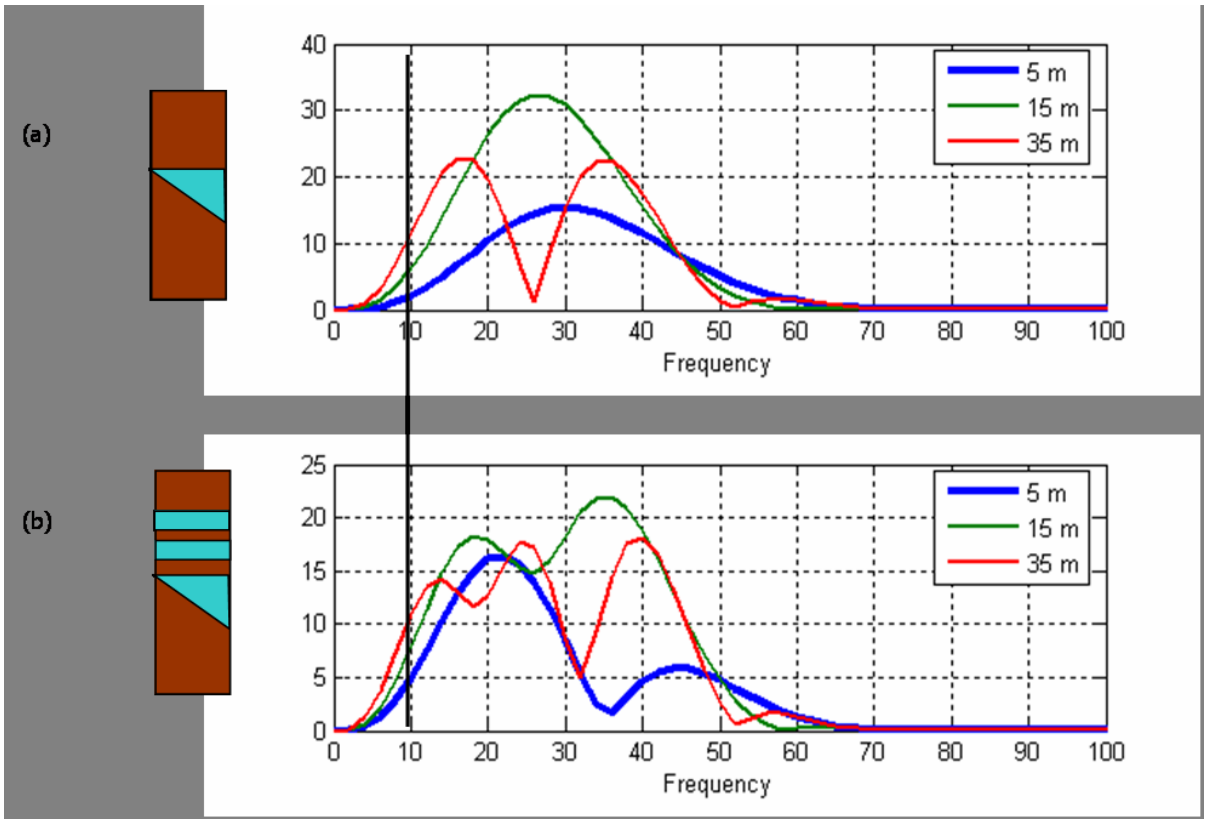

Figure 30. Windowed Fourier Transform amplitude spectra for three synthetic traces with difference sand thickness. The WFT amplitudes in Figures 3 and 4 are picked at 10 Hz as marked by a vertical line

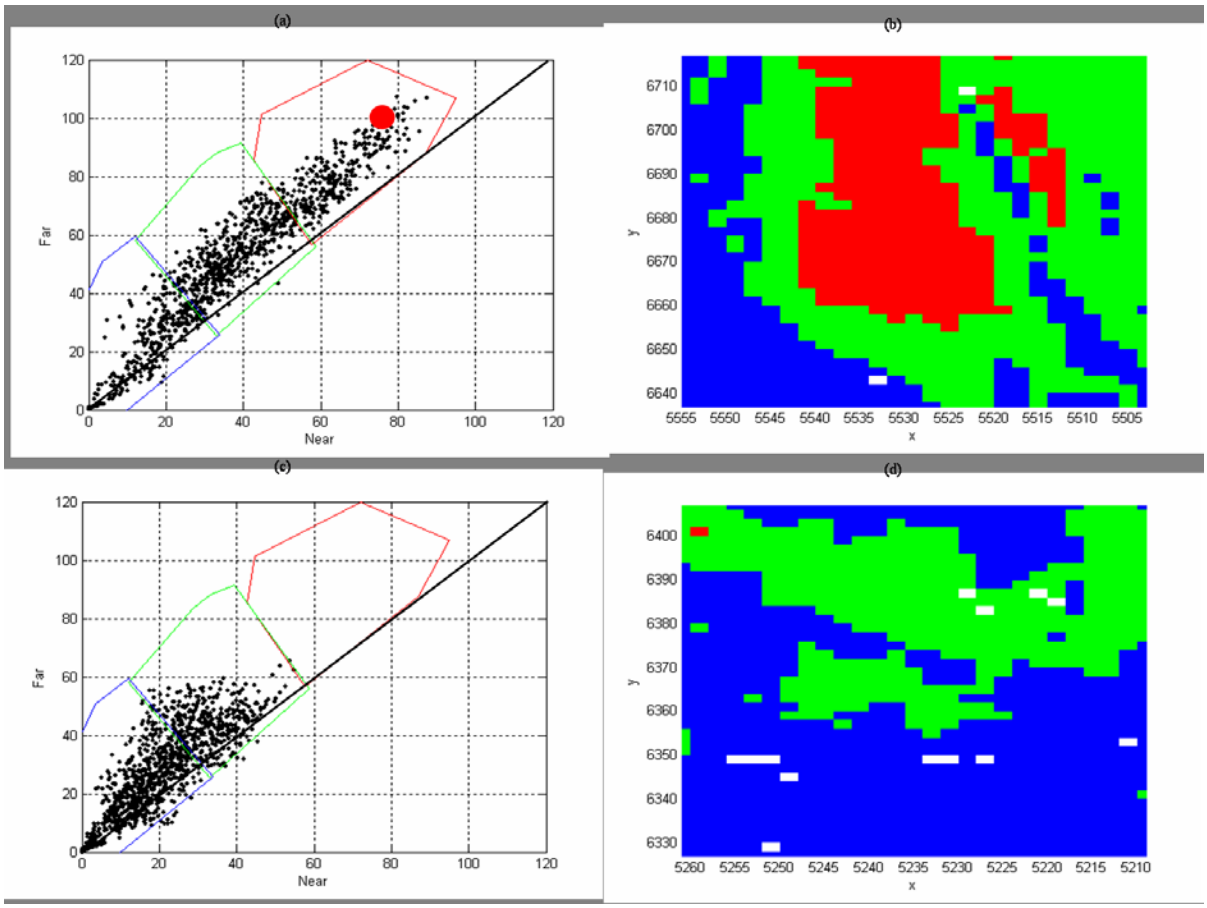

Figure 31. Field data example. (a) Crossplot of near and far WFT amplitudes at 10 HZ for Patch A; (b) Classification based on (a); (c) and (d) are the classification for Patch B. The red dot in (a) indicates the King Kong well location

Application/Conclusions

An interpretation of the Ursa field was made by Hilterman (2001). In his interpretation he identified a fizz gas saturated reservoir interval which can be seen in well log outcrop and seismic data in figure 13. The AVO response can be seen in Figure 14 for the upper fizz gas interval. This response shows very little change in seismic response which is consistent with log data but not seismic data. The seismic response shows a bright spot but when compared to well log data in that interval we see that there is no hydrocarbon indication from resistivity logs and the gamma shows no sign of reservoir quality sand. The well log has a slight fining upward sequence which indicates the presence of thin beds. A stated earlier in the paper thin beds are interpreted to include levee, inter-channel and outer fan fringe deposits and are composed of fine grained sands or silt and graded beds. The presence of thin beds causes a possible pay zone to be overlooked. By

combining well log response, seismic expression and outcrop information we can make a more accurate interpretation by using what we know about deep water sediments in outcrop to extend to the interpretation into areas that may not have adequate well control to make the interpretation for sub seismic scale features. The use of outcrops as analogues acts as a visual aid and model constraint for improving seismic interpretation of deepwater sediments.

Plans

We plan to continue our efforts, not only in research but in communications as well. Although we have not obtained all the data sets yet, we do have several examples to test our concepts with frequency content, attenuation, and thin bed effects. The Ursa dataset is particularly rich, containing both economic and non-economic ("Fizz Gas") hydrocarbons.

Our second mini-forum on direct hydrocarbon indicators ("What's New in DHI") was held June 15 at the University of Houston. We received numerous complements and positive comments on the meeting. This has been a very good method to both show the results of this DOE project as well as simulate exchange of ideas about the topic in general. We will include a detailed summary of the symposium in the next quarterly report.

Meanwhile, expected individual tasks for next period are as below:

D. Han (UH) - Summarize Direct Hydrocarbon Indicator mini-symposium
- Begin analysis of data from Kerr McGee for Nansen field
- compare measurements with log analysis
- Collate sample data
- Make additional ultrasonic measurements on sands

R. Gibson (TAMU) - Modify modeling schemes to include local 1/Q values
- Continue analysis of seismic data
- Continue forward modeling with site-specific parameters
-Specify and transfer seismic data from Veritas

M. Batzle (CSM) - Assist with Direct Hydrocarbon Ind. Mini-symposium
& K. Baker - Continue geologic analysis
- Continue log data analysis
- Continue measurements on Troika samples

Duane Dopkin or Huw James (Paradigm)
- Test reprocessing sequence on Viking Graben data
- Evaluate frequency response versus NMO
- Perform standard AVO analysis with different processing

Further information can be obtained from:

Dr. Michael Batzle

Colorado School of Mines

Phone: 303-384-2067 email: mbatzle@mines.edu

References

Anderson, Donna. Colorado School of Mines Lewis Consortium Field Trip Guide: Delta-Front to slope sediment delivery into the basin. July 31-August 1, 2004.

AAPG memoir 26 Seismic Stratigraphy-Applications to hydrocarbon Exploration 1977
Borer, Jim. Personal Communication. July 20, 2004.

Chapin , M. A., P. Davies, J.L. Gibson, H.S. Pettingill, 1994, reservoir Architecture of turbidite sheet sandstones in laterally extensive outcrops, Ross formation western Ireland, in Paul Weimer and B.F. Perkins Eds., Submarine Fans and turbidite Systems, Gulf Coast Section-SEPM Foundation 15th annual research Conference, 53-68.

Dechesne, Marieke. Personal Communication. July 20, 2004.

Gardner, M.H., and Batzle, M., 2003 Lithology and Fluids: Seismic Models of the Brushy Canyon Formation West Texas

Gardner, M.H., et al. 2003, Stratigraphic Process Response model for submarine channels and related features from studies of Permian Brushy Canyon outcrops, West Texas: Marine and Petroleum Geology, 20, 757-787.

Gardner. H., Borer, J.M., 2000, Submarine channel architecture along a slope to basin profile, Brushy Canyon Formation, West Texas, in A.H. bouma and CG Stone, eds., Fine-Grained turbidite systems, AAPG Memoir 72/SEPM Special Publication No. 68, p 195-214.

Gardner, M.H., June 29, 2004. Slope and Basin Consortium Website Colorado School of Mines: Resource Optimization of Slope and Basin Reservoirs through Enhanced Imaging of Reservoir Architecture http://www.mines.edu/Academic/geology/sbc/index.shtml

Gassmann, F., 1951, Uber die Elastizitat poroser medien. Veri der nature Gesellshaft Zurich, 96, 1-23.

Hilterman, F. Seismic Amplitude Interpretation 2001 Distinguished Instructor Short Course Series no. 4 EAGE 2001

Keys Robert G and Foster Douglas J. Comparison of Seismic Inversion methods on a Single real data Set. SEG 1998

Meckel, L.D., et al. Genetic Stratigraphy Architecture and Reservoir Stacking Patterns for Upper Miocene-Lower Pliocene Greater Mars-Ursa Intraslope Basin Mississippi Canyon, Gulf of Mexico. 22nd Annual gulf Coast Section SEPM Foundation Bob F

Perkins research Conference-2002. pp. 113-146.

Mutti and Normark, 1987, Comparing examples of modern and anchient turbidite systems: problems and concepts, in J.K. Leggett and GG Zuffa, eds., Marine Clastic Sedimentology: London Grahm and Trotman, 1-38.

B. E. Prather,2 J. R. Booth,3 G. S. Steffens,4 and P. A. Craig , Pages 701 - 728 , Volume 82 (1998) Classification, Lithologic Calibration, and Stratigraphic Succession of Seismic Facies of Intraslope Basins, Deep-Water Gulf of Mexico. 1998. AAPG Bulletin

Reynolds, M. W., 1976, Influence of recurrent Laramide structural growth on sedimentation and petroleum accumulation, Lost Soldier area, Wyoming: AAPG Bulletin, v. 60, p. 12-33

Slatt, R.M., 2005, AAPG/SEg Spring Student Expo: Petroleum geology of Deepwater Turbidite Depositional Systems Short Course Notes, Hosted by School of geology and Geophysics university of Oklahoma. March 10-12, 2005.

Appendix A

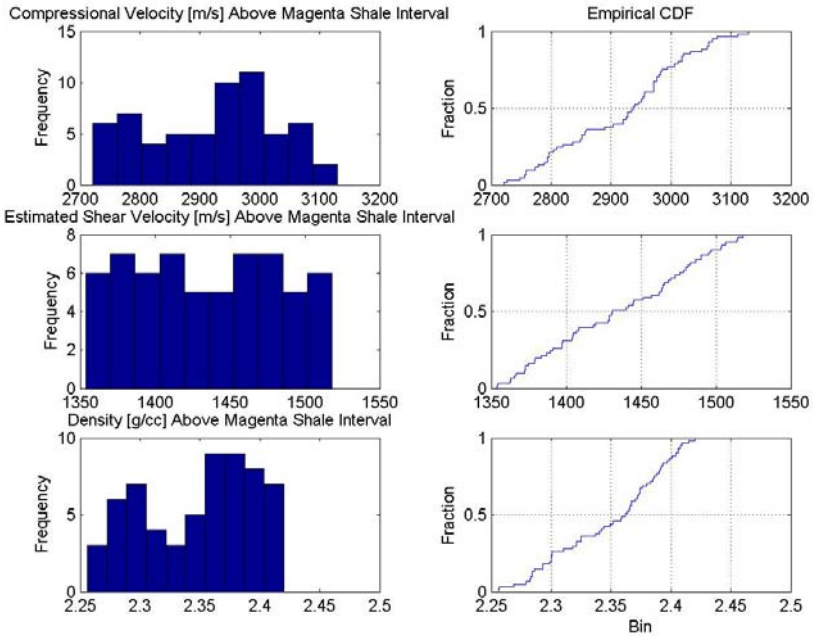

Histograms and empirical CDF curves for VP, estimated Vs and Density for the Above Magenta Shale interval

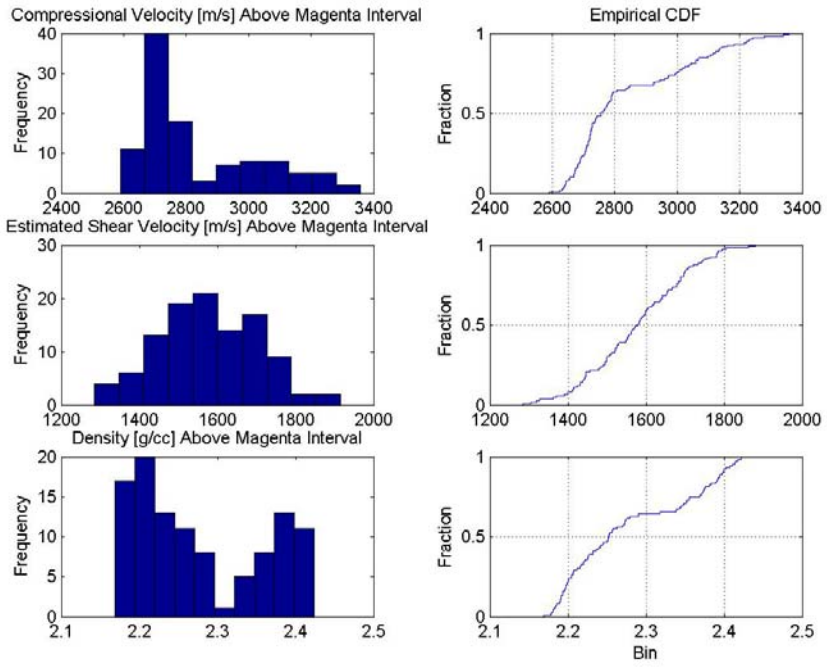

Histograms and empirical CDF curves for VP, estimated Vs and Density for the Above Magenta reservoir interval

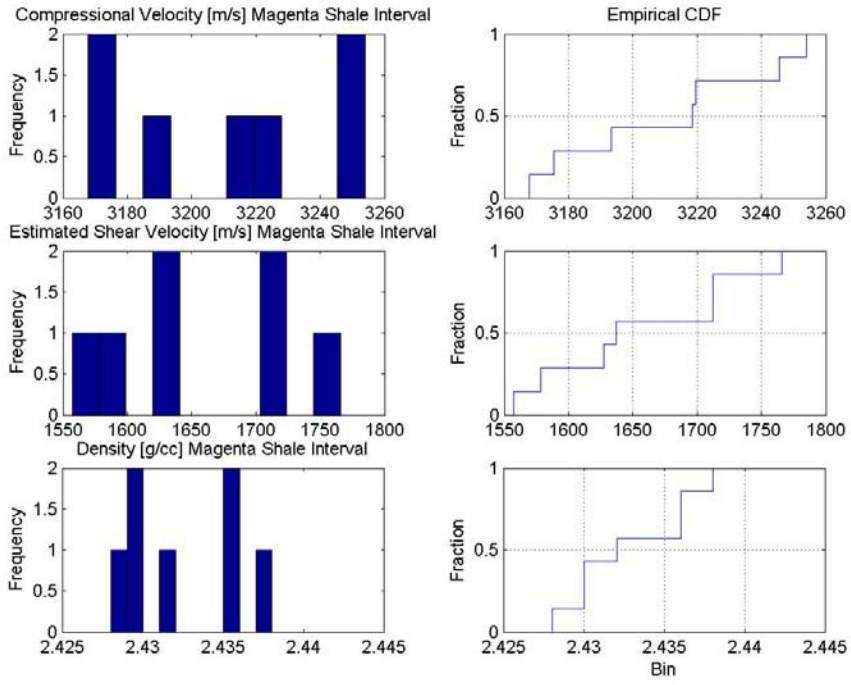

Histograms and empirical CDF curves for VP, estimated Vs and Density for the Magenta Shale Interval

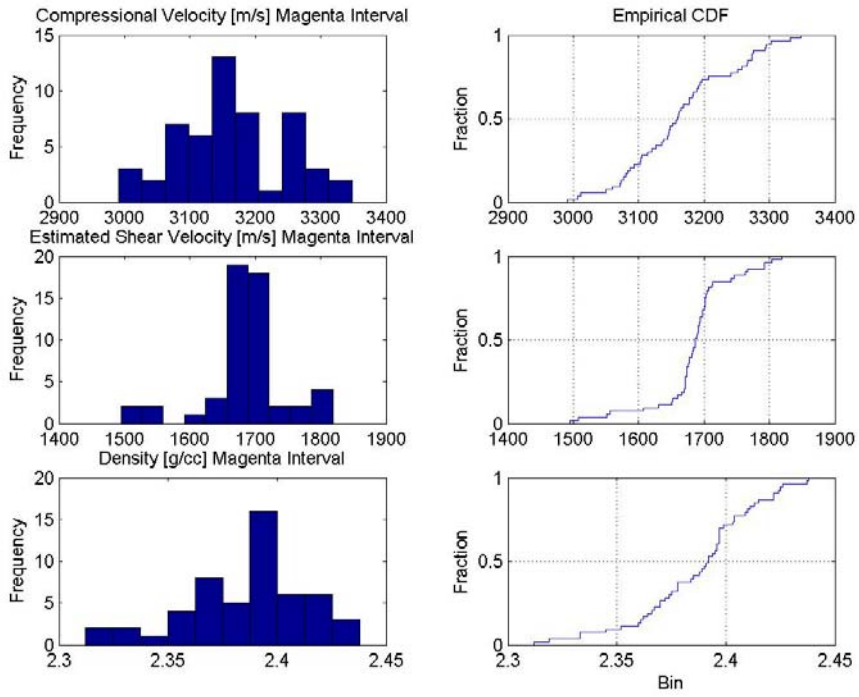

Histograms and empirical CDF curves for VP, estimated Vs and Density for the Magenta Reservoir interval

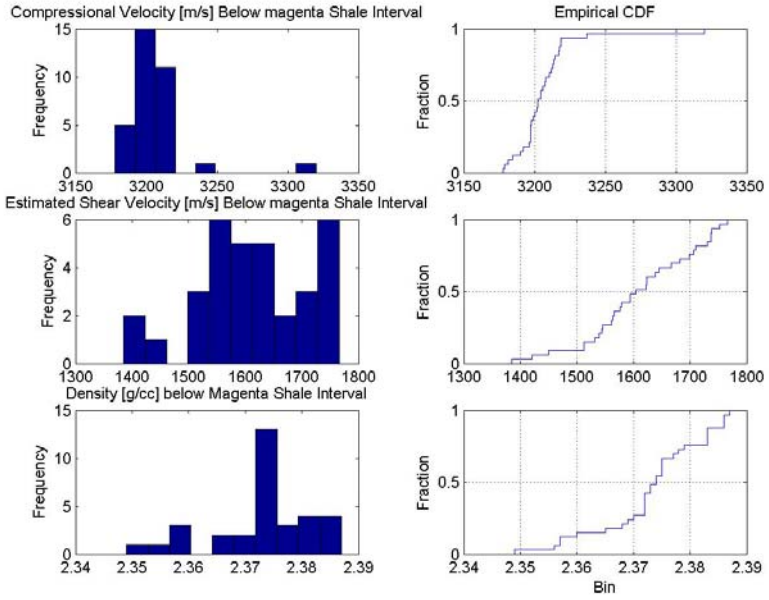

Histograms and empirical CDF curves for VP, estimated Vs and Density for the Below Magenta Shale interval

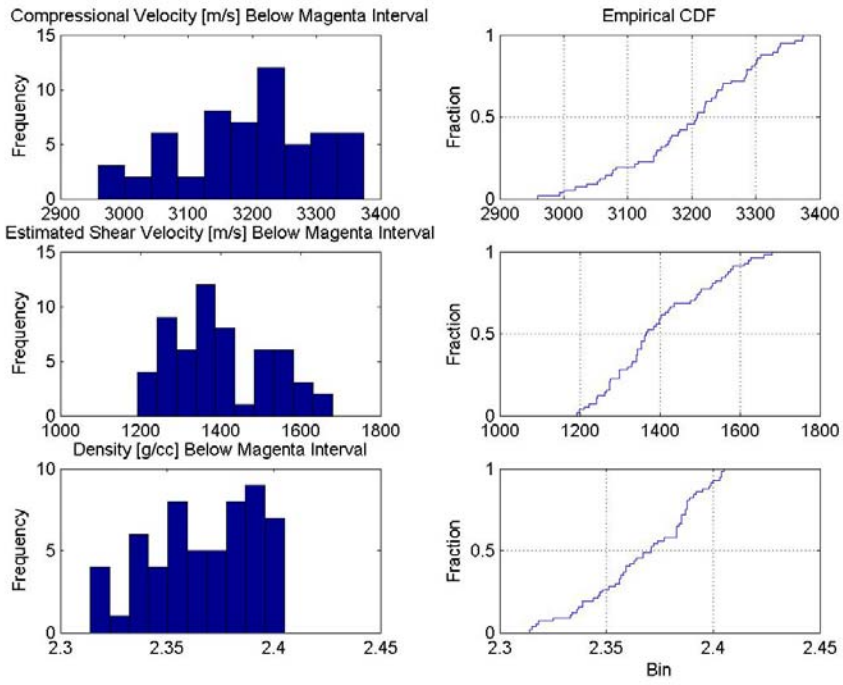

Histograms and empirical CDF curves for VP, estimated Vs and Density for the Below Magenta Reservoir interval

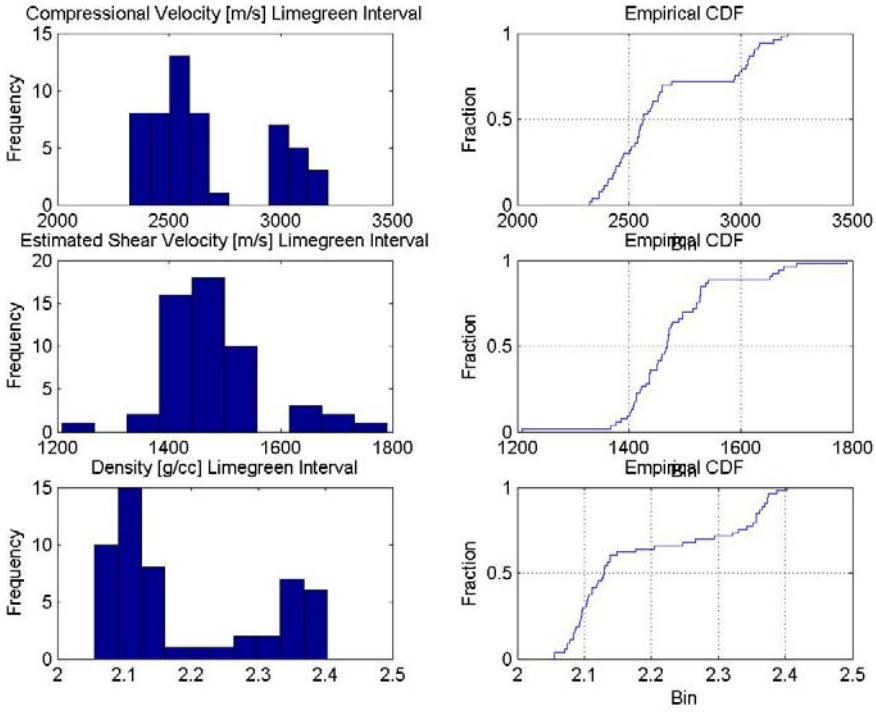

Histograms and empirical CDF curves for VP, estimated Vs and Density for the Limegreen Shale interval

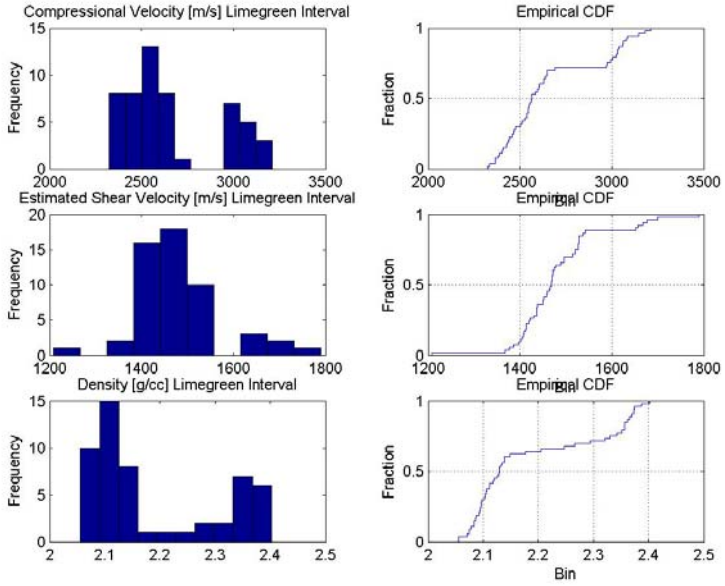

Histograms and empirical CDF curves for VP, estimated Vs and Density for the Limegreen reservoir interval

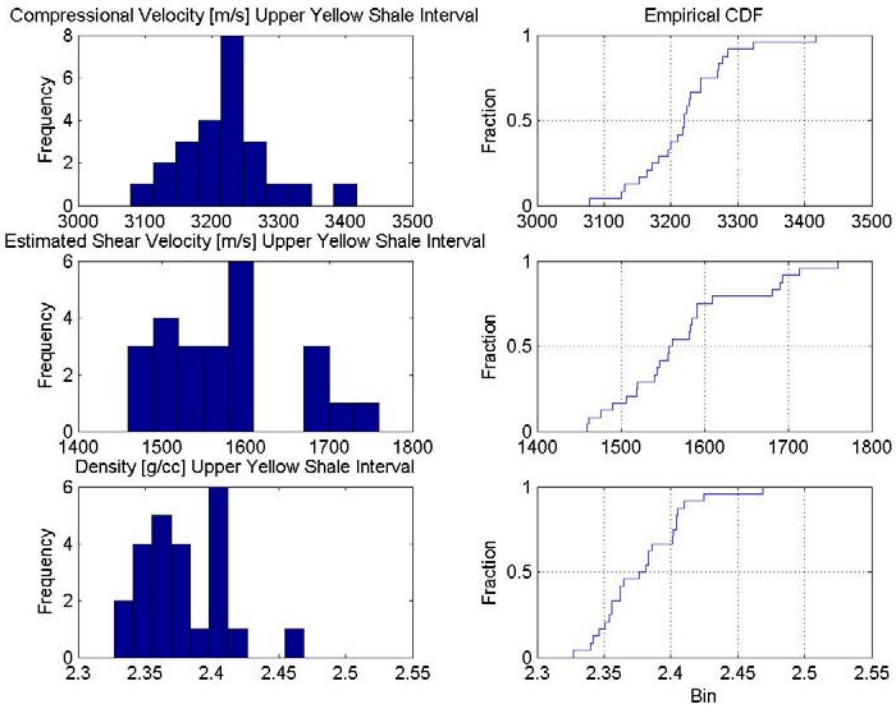

Histograms and empirical CDF curves for VP, estimated Vs and Density for the Upperyellow shale interval

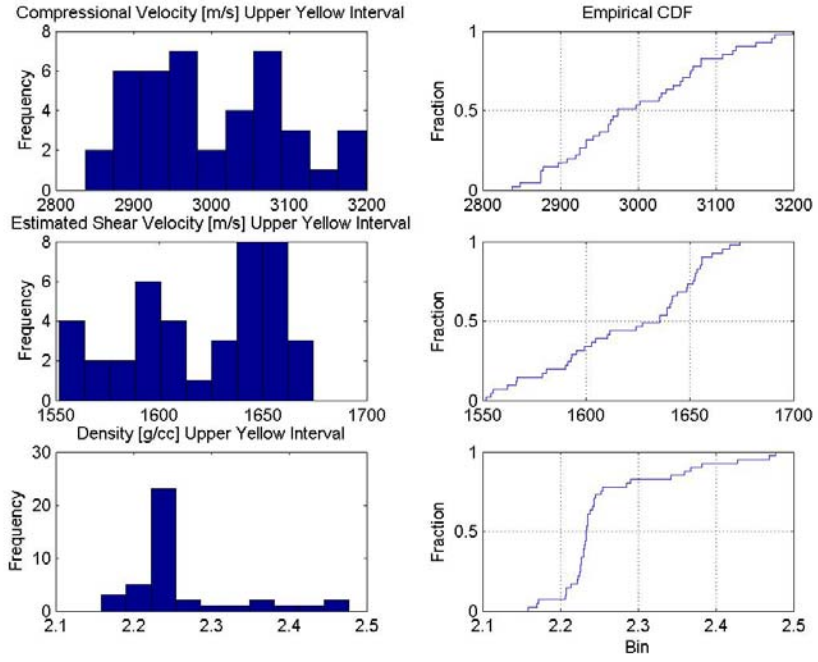

Histograms and empirical CDF curves for VP, estimated Vs and Density for the Upperyellow Shale interval

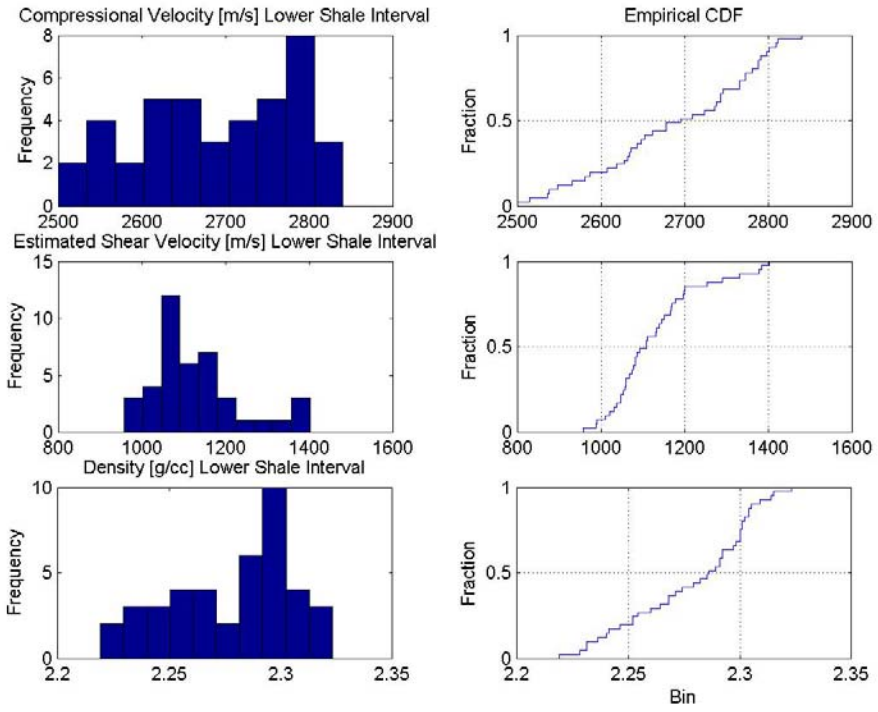

Histograms and empirical CDF curves for VP, estimated Vs and Density for the loweryellow shale interval

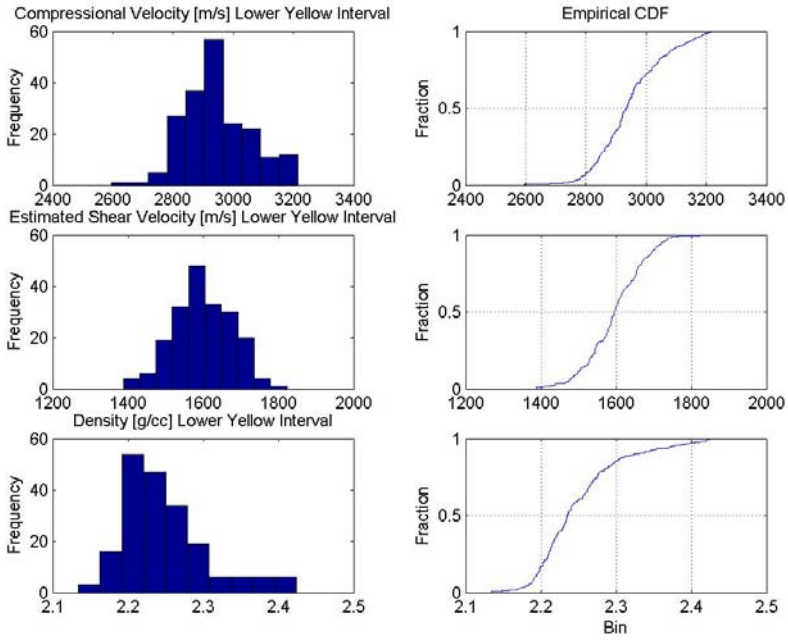

Histograms and empirical CDF curves for VP, estimated Vs and Density for the Lower yellowreservoir interval